The Effects of Resonance Decays on Particle Ratios and Momentum Spectra

David T. Brookes

July 1997

The Effects of Resonance Decays on Particle Ratios and Momentum Spectra

David Thomas Brookes

Department of Physics
University of Cape Town
Rondebosch 7700
South Africa

Abstract

A Hadron Gas model, including resonance decays, is used to predict momentum spectra and particle ratios. The model, including all significant two and three body resonance decays, is compared with transverse momentum spectra from the CERN-SPS NA44 Pb–Pb experiment and the implications of the fits are discussed. It is shown that resonance decays fail to explain the low m_T anomaly in the pion transverse momentum spectrum. The effects of resonance decays are then considered in the calculation of various particle ratios. The width of the rapidity window is varied and its effect on the particle ratios is examined.

Thesis submitted in fulfilment of
the requirements for the degree of Master of Science
at the University of Cape Town.

Research supported by the Foundation for Research and Development.

Contents

List of Figures

List of Tables

Chapter 1

Models of relativistic heavy ion collisions and signals of quark-gluon plasma

1.1 Introduction

The goal of ultra-relativistic heavy ion collisions, is to probe the nature of hadrons and gain insight into the origins of the Universe, through the production of a quark-gluon plasma (or QGP for short). A QGP is a state of quark deconfinement caused by the collision of two ultra-relativistic nuclei. In such a collision the participating nucleons are squashed so close together that the quarks which constitute them are essentially free to move around without being restrained to the individual protons and neutrons from which they came. This state, a new phase of matter, is predicted both by lattice QCD and by the MIT bag model. The order of the phase change is still the subject of detailed investigation.

If a QGP is indeed formed, not only will these predictions be verified, striking a blow for the Standard Model, but a completely new phase of matter will be observed. The hope is that new physics will be revealed and in particular, we hope to learn more about how quarks interact. Furthermore, QCD predicts a restoration of chiral symmetry where the quark masses drop to zero. Finally, one can speculate that the primordial universe was once (for a short time) a massive soup of quarks and gluons. It is as though we are trying to create a miniature "big bang" in the laboratory in order to probe the origins of our Universe (see figure 1.1).

The two main centres where these experiments are being conducted are the Brookhaven National Laboratory (BNL) in the United States and the European Centre for Nuclear

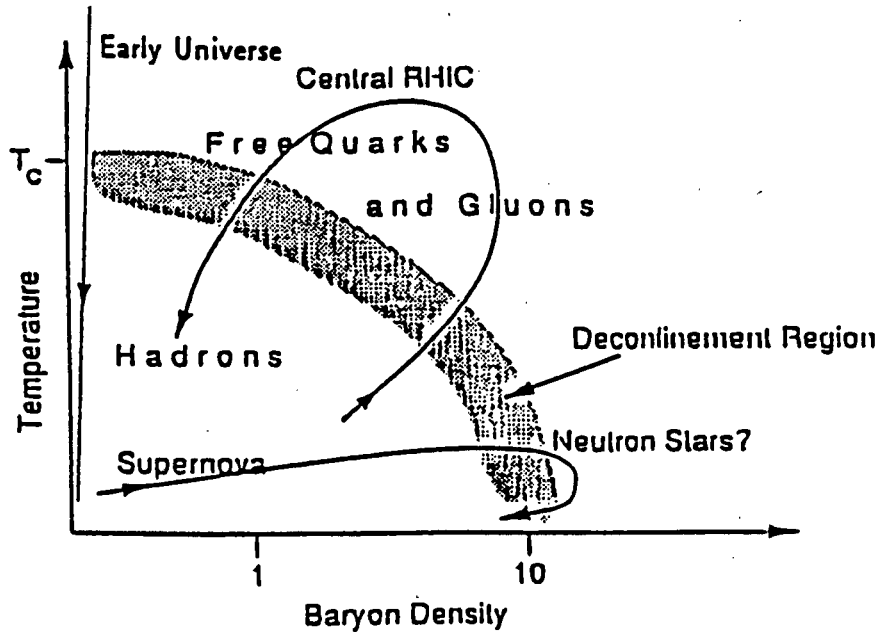

Figure 1.1: A phase diagram for nuclear matter, illustrating how a transition from hadrons to free quarks may occur at both high temperatures and low densities (conditions which may have existed in the early universe) on the one hand and on the other hand, at low temperatures and high densities (such as the centre of a neutron star [18].)

Research (CERN) in Switzerland. The first round of collisions involving light ions such as oxygen and sulphur were conducted in the 80's and 90's and reached the energy densities at which a phase transition is predicted to occur, but seemed to fail to produce clear signs of a QGP. The second round of collisions has used heavier ions; 10 GeV/u Au–Au collisions at the AGS (at BNL) in 1992 and 160 GeV/u Pb–Pb collisions at the SPS (at CERN) in 1994 and 1996. The results of these experiments are still being analysed, but the most promising results appear to come from the SPS Pb–Pb experiment.

All these experiments involve a projectile beam colliding with a stationary target and thus a beam energy of 160 GeV per nucleon translates to a centre of mass (CM) energy of about 9 GeV/u (see appendix B). Clearly it is far more efficient to collide two beams of heavy nuclei head on, and in the quest for even higher energies, the next round of experiments will do just that. The relativistic heavy ion collider (or RHIC) at BNL is due to come on line in 1998 and will collide uranium ions at energies of 200 GeV/u in the CM frame. In about 2010 CERN is due to finish the conversion of its LEP ring into a large hadron collider (LHC) which will collide heavy nuclei at considerably larger (6300 GeV/u) centre of mass energies.

With the predictions that the strong, weak and electromagnetic coupling constants will only unite at energies of the order of 10^{15} GeV, it is possible that these experiments will find themselves stranded in the middle of a desert with no new physics in sight, but

few believe this. Physicists are pinning their hopes on observing new physics from each successive round of ultra-relativisic heavy ion collisions. There can be little doubt that physics is in need of new data: quantum chromodynamics, the model of quark interactions, is in need of refinement as it is still not clear how quarks interact. By placing them in a state of deconfinement, we hope to observe the predicted phase change and to understand a little better the nature of the strong force. It cannot really be predicted what will happen as energies increase; energy densities at which deconfinement is predicted to occur may have been surpassed, and a QGP may very well have been formed, yet there seem to be no clear, uncontested signals. Nature has been extremely reticent in revealing any new secrets. Part of the problem that faces us, is knowing where and how to look for new phenomena.

1.2 Models

Models of heavy ion collisions can be divided into two broad categories; namely: phenomenological, macroscopic models and microscopic models. This thesis intends to focus on a phenomenological approach, examining models of the collective interaction and motion of a system after a heavy ion collision. Particle ratios and momentum spectra, will be predicted using a Hadron Gas model [6, 9, 17], extended to include resonance decays. The formulation of a stationary Hadron Gas model will be discussed in detail in chapter 2 and extensions of the model to include hydrodynamical flow and resonance decays will be covered in chapters 3 and 4 respectively. In chapter 5 the low transverse momentum anomaly in the pion momentum spectrum will be examined. A stationary Hadron Gas model, including a full spectrum of two and three body resonance decays, will be compared with the results from the NA44 Pb–Pb experiment conducted at CERN. Chapter 6 will examine the effects of resonance decays and the width of the rapidity window on the theoretical prediction of particle ratios.

The phenomenological approach may seem puzzling at first. Rather than trying to model the QGP phase and the nature of the interactions, phenomenological models tend to ignore the fact that a QGP may have been formed and use the existing tools at our disposal to model the system on a macroscopic level. Within a statistical framework, we hope to observe deviations from the expected behaviour rather than see startling agreement. If the model is extremely successful on the other hand, we must ask why this model, which ignores the existence of a QGP, manages to fit the data. Answering such questions will ultimately enhance our understanding. If a phenomenological model is successful, we hope that it will reveal the nature of the interaction in the few fractions of a second after a collision. It may very well turn out that the success of a particular model fits in very well with the possibility of QGP formation, but this is open to debate

and speculation — which is the very essence of this approach.

1.3 Signatures

Not only do we try to model the short-lived QGP phase and the particles which emanate from it, but we are also searching for clear signals that quark matter has been formed. These signals must somehow pass through the large gas of freeze-out hadrons which hide the QGP from our view. In this class, dileptons and photons, which do not interact strongly but rather electromagnetically, can pass straight through to the detectors and may carry memory of the QGP from which they possibly came. It has also been predicted that the formation of a QGP will lead to the suppression of some hadrons and the enhancement of others. A brief review of some proposed signals of QGP is given below.

1.3.1 Photons and dileptons

Since photons and lepton pairs only interact electromagnetically, they are a potentially useful probe into the heart of a heavy ion collision. Their mean free path can be shown to be much longer than the transverse size of the collision volume [2]. Direct photons produced in such processes as $gq \rightarrow \gamma q$ and $q\bar{q} \rightarrow \gamma g$, will carry a memory of the temperature of the QGP [7] *provided* that they can be distinguished from photons emanating from hadronic decays.

Lepton pairs are produced at all stages in the collision process from such varying sources as $q\bar{q}$ annihilation to hadronic decays. Thus a careful study of lepton pairs can map the whole space-time history of the collision from QGP to freeze-out [2]. A clear case of enhanced dilepton production can be seen in figure 1.2 which plots the experimental e^+e^- mass spectrum against a theoretical mass spectrum of e^+e^- pairs from hadronic decays such as $\omega \rightarrow ee\pi^\circ$ and $\rho/\omega/\phi \rightarrow ee$. It is clear from the large deviation of the experiment from the theory that there must be additional mechanisms involved in the production of e^+e^- pairs. This could be an indication of the formation of a QGP where a process like $q\bar{q} \rightarrow e^+e^-$ would predominate.

1.3.2 Strangeness enhancement

Two mechanisms are at work in a QGP which will promote the production of $s\bar{s}$ pairs.

1. There is a predominance of u and d valence quarks and gluons, which implies a large chemical potential, making it increasingly difficult to add more u and d quarks. In

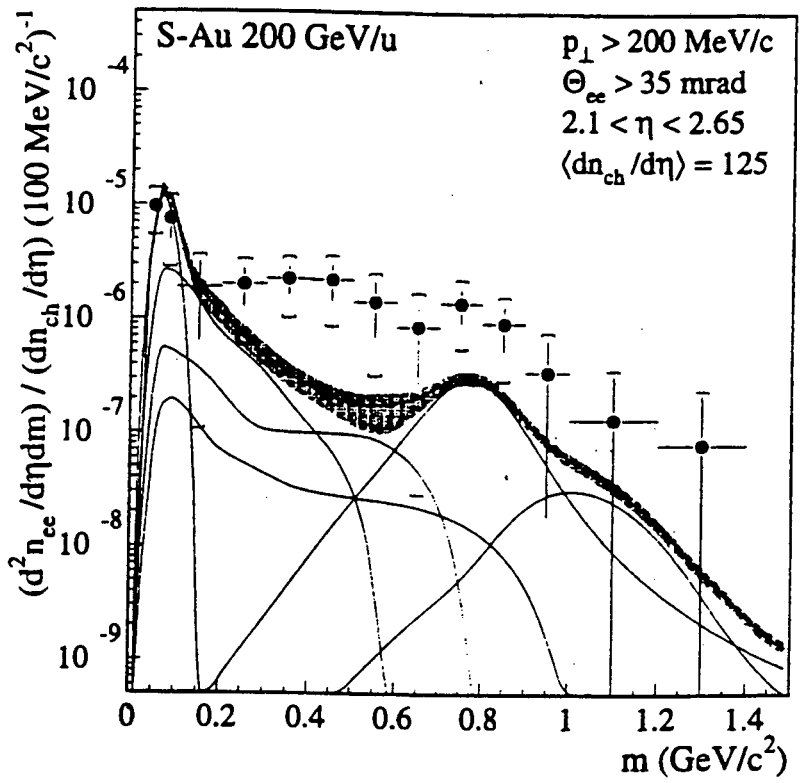

Figure 1.2: The total e^+e^- mass spectrum from 200 GeV/nucleon S–Au collisions [2]. The experimental data is placed against a background of known hadronic decays.

addition, the large number of u and d quarks will lead to increased Pauli blocking as the available phase space is filled up.

2. QCD predicts that the strange quark mass will change from a "constituent" quark mass to a small "current-algebra" mass.

A better way to understand this is to think rather of strangeness suppression [31]. If a QGP is formed, the mechanisms that encourage the production of strange quarks ensure that the strange quarks quickly reach chemical equilibrium. If only a gas of hadrons is formed, the threshold for the production of strange hadrons is much higher than the threshold for the production of $s\bar{s}$ pairs (simply because the strange hadrons are heavier). Thus, in a hadron gas, strange hadrons will be produced too slowly to reach chemical equilibrium before freeze-out, hence a strangeness suppression. Several experiments have revealed clear signals of strangeness enhancement.

1.3.3 J/Ψ suppression

J/Ψ suppression was proposed by Matsui and Satz [8] in terms of the mechanism for quark deconfinement, namely the Debye screening of the quark colour charge. $C\bar{C}$ pairs

produced in a heavy ion collision which find themselves in the deconfined environment of a QGP, will be prevented from forming charmonium by the screening effect and the charmed quark and its anti-charm partner will head off in separate directions, forming charmed mesons such as: $c\bar{u}$ and $\bar{c}u$ etc ... (On the most simplistic level: the predominance of u and d quarks destroy the $c\bar{c}$ pair and they are carried apart, never to meet again). The latest data from the 1994 CERN Pb–Pb experiment presents some of the most convincing evidence for the formation of a QGP [14].

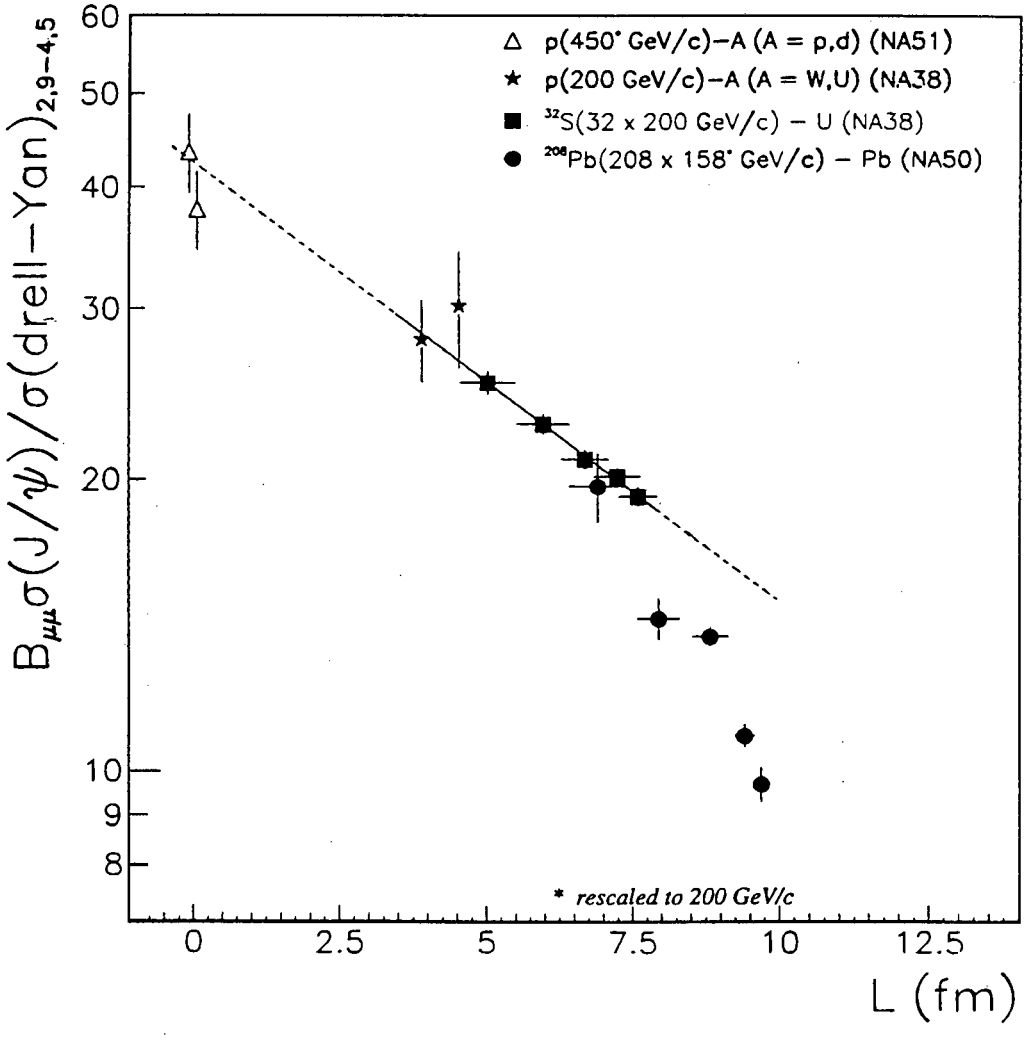

Figure 1.3: A plot, demonstrating J/Ψ suppression as a function of length of nuclear matter. Note how the J/Ψ is suppressed by absorption by nuclear matter and follows this trend, until dropping off very steeply. This sudden plunge is observed in NA50 Pb–Pb data and is some of the strongest evidence in support of the formation of a QGP

Chapter 2

The Hadron Gas model

2.1 Introduction

The Hadron Gas model [6, 9, 17] treats the fireball resulting from a heavy ion collision and the freeze-out hadrons that arise from it, as a statistical gas. The fundamental assumption is that the particles which constitute the gas have undergone enough collisions with each other to be thermally equilibrated. The possibility that the gas of hadrons could come from one or maybe two distinct thermal sources is of fundamental importance and will be discussed in the conclusion to this chapter.

The model is built up, starting from the Lorentz invariant momentum spectrum of a gas of a particular species of particle coming from a stationary thermal source at temperature T:

$$E\frac{d^3N}{d^3p} = \frac{gV}{(2\pi)^3}E\frac{1}{e^{(E-\mu)/T} \pm 1} .$$

Here g is the spin-isospin degeneracy factor for the species in question, $f(E,\mu) = (e^{(E-\mu)/T} \pm 1)^{-1}$ is the Bose or Fermi partition function denoting the thermal average occupancy of a particular energy level [15], $V/(2\pi)^3$ is the density of energy levels in phase space and the grand canonical chemical potential, $\mu = B\mu_B + S\mu_S$, depends on the baryon and strangeness quantum numbers B and S respectively. Because of the high temperatures involved we can make the Boltzmann approximation, giving:

$$E\frac{d^3N}{d^3p} = \frac{gV}{(2\pi)^3}Ee^{-(E-\mu)/T} . \tag{2.1}$$

2.2 Cylindrical coordinates

The high momenta of the colliding nuclei result in a fireball which is expanding more strongly in the longitudinal direction (ie: in the direction from which the nuclei came) than in the transverse direction. The resulting fireball can be seen to be expanding in a long cylindrical tube and it is therefore convenient to introduce cylindrical coordinates, namely: longitudinal rapidity, y, and transverse mass, m_T. (see appendix A for a full treatment.)

We can now convert d^3p into cylindrical coordinates: (see appendix C)

$$d^3p = 2\pi m_T dm_T E dy \ ,$$

and substituted into equation 2.1 (along with $E = m_T \cosh y$), this yields

$$\frac{d^2N}{dy m_T dm_T} = \frac{gV}{(2\pi)^2} e^{\mu/T} m_T \cosh y e^{(-m_T/T)\cosh y} \ . \tag{2.2}$$

Note that a central collision has been assumed and thus cylindrical symmetry can be invoked. The angle ϕ has accordingly been integrated out.

2.3 The transverse momentum spectrum

From equation 2.2 we can obtain the transverse momentum spectrum $dN/m_T dm_T$ by integrating out the rapidity:

$$\frac{dN}{m_T dm_T} = \frac{gV}{2\pi^2} m_T e^{\mu/T} K_1\left(\frac{m_T}{T}\right) \ ,$$

which tends to the following limit when we consider $m_T \gg T$:

$$\lim_{\frac{m_T}{T}\to\infty} \frac{dN}{m_T dm_T} \ \alpha \ \sqrt{m_T} e^{-m_T/T} \ .$$

(See appendix D for a full derivation.)

Taking into account that some of the experiments conducted use a small rapidity window, it can be shown that

$$\frac{dN}{m_T dm_T} \ \alpha \ e^{-m_T/T} \ .$$

Thus a logarithmic plot of the transverse momentum spectra of various paticle species: $dN/m_T dm_T$ vs $m_T - m_0$ should be fitted well by a straight line of slope: $-1/T$. Figure 2.1 reveals that several particle species clearly follow a Boltzmann distribution, but a straight line fails to fit the pion momentum spectrum. There is a clear anomaly at low m_T where

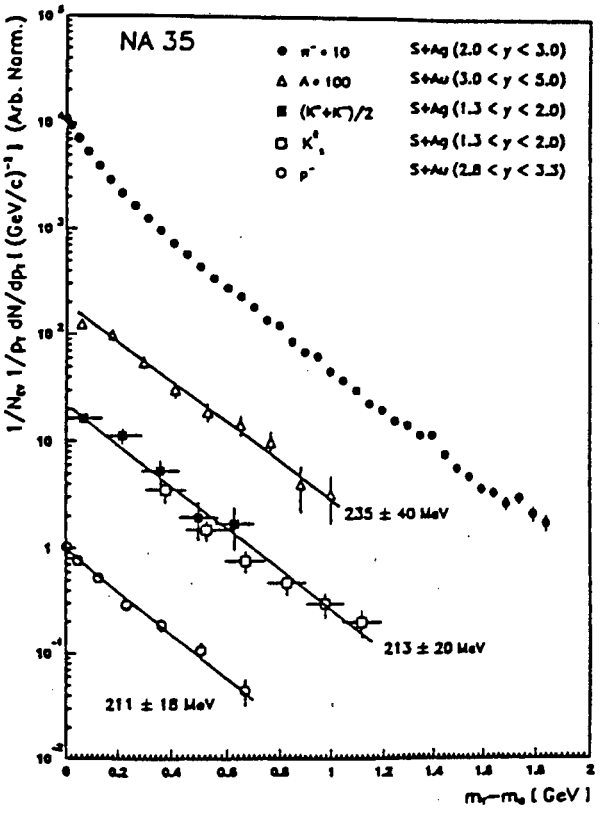

Figure 2.1: A plot of $dN/(m_T dm_T)$ against $m_T - m_0$ [10]. All the spectra are fitted well by the simple thermal model which has been developed, apart from the π^- spectrum which shows a marked anomaly at low m_T

the tail of the graph is significantly steeper than the theory predicts. The high m_T tail is also problematic in that it is slightly flatter than we would expect with the thermal picture developed so far. These anomalies can possibly be accounted for by considering transverse flow and by including pions emanating from resonance decays. Since some of the resonance momentum is shared with other decay products, there is a glut of resonance pions with lower transverse momenta which causes a significant rise in the slope at low m_T while transverse flow will boost the high m_T part of the spectrum. Figure 2.2 reveals how resonance pions outgrow thermal pions at typical QGP temperatures and baryon densities, and thus resonance decays cannot be ignored [17]. The inclusion of resonances and other simple improvements to the hadron gas model will be much of the focus of the remaining chapters of this thesis.

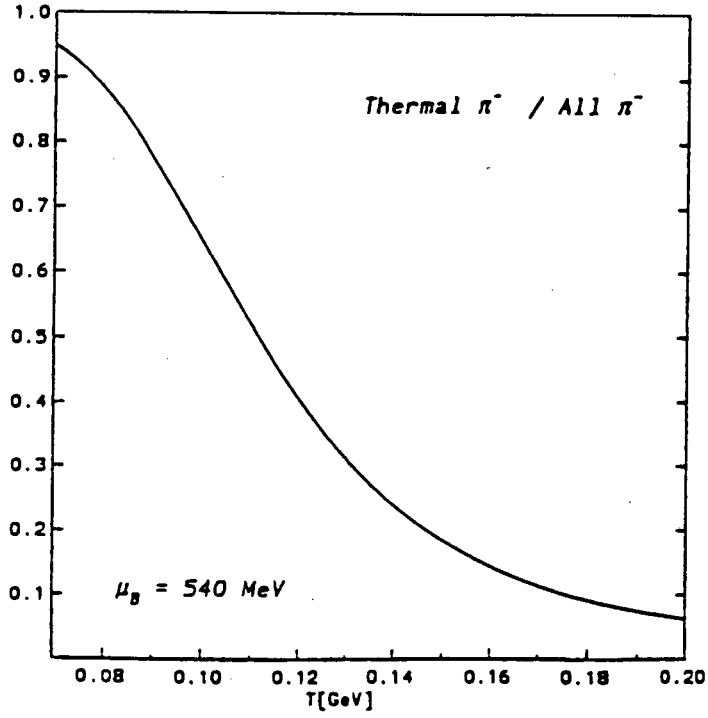

Figure 2.2: Thermal vs resonance pions, demonstrating how resonance decay pions dominate the total pion population at temperatures of 150–200MeV at typical BNL AGS baryon densities [17].

2.4 The longitudinal momentum spectrum

As with the transverse momentum spectum we begin with equation 2.2, but now we integrate out m_T, leaving the rapidity spectrum for a single, stationary thermal source:

$$\frac{dN_{th}}{dy} = \frac{gV\cosh y}{(2\pi)^2} e^{\mu/T} \int_{m_0}^{\infty} m_T^2 e^{-\alpha m_T} dm_T \ , \tag{2.3}$$

where $\alpha = \cosh y/T$. Equation 2.3 may be integrated by parts twice to yield:

$$\frac{dN_{th}}{dy} = \frac{gV}{(2\pi)^2} e^{\mu/T} \exp\left(\frac{-m\cosh y}{T}\right) T^3 \left(\frac{m^2}{T^2} + \frac{m}{T}\frac{2}{\cosh y} + \frac{2}{\cosh^2 y}\right) . \tag{2.4}$$

For light particles (eg: pions) where $m \leq T$ equation 2.4 reduces to $dN/dy \ \alpha \ \cosh^{-2}(y - y_{FB})$, which approximates a Gaussian distribution with width: $\Gamma_{fwhm} = 1.76$. Rewriting equation 2.4 as

$$\frac{dN_{th}}{dy} = \frac{gV}{(2\pi)^2} e^{\mu/T} \exp\left(\frac{-m\cosh y}{T}\right) m^2 T \left(1 + \frac{T}{m}\frac{2}{\cosh y} + \left(\frac{T}{m}\right)^2 \frac{2}{\cosh^2 y}\right) ,$$

it can be shown that for $m \geq T$ this equation behaves like a Gaussian, centred about the rapidity of the fireball y_{FB}:

$$\frac{dN_{th}}{dy} \ \alpha \ \exp\left(\frac{-m}{2T}(y - y_{FB})^2\right) .$$

This has a mass dependent width which narrows like $1/\sqrt{m}$ as particle masses increase:

$$\Gamma_{fwhm} = \sqrt{8 \ln 2}\sqrt{\frac{T}{m}} .$$

Figure 2.3 shows a comparison of these theoretical curves (the dotted lines) with rapidity spectra from the NA35 S+S 200 GeV/u experiment. It is clear from the figure that the distribution from a stationary thermal source completely fails to fit the data. Particularly alarming is the proton rapidity distribution which exhibits what is termed "nuclear transparency". Two "humps" of protons with disproportionately high rapidity can clearly be seen. This seems to indicate that the two colliding nuclei pass almost straight through each other, leaving a trail of particles behind them. This nuclear transparency is one of the main obstacles to reaching energy densities high enough to induce the proposed phase change. It has led to a shift to colliding even heavier nuclei such as Pb in order to overcome the problem.

2.5 Spectra from flowing sources

2.5.1 Longitudinal flow

Referring to figure 2.3, it is clear that all rapidity spectra are wider than a naive stationary thermal source would predict. Without carrying out the complicated calculations, it is easy to argue that inclusion of resonance decays in the π^- spectrum (for instance) would only worsen the fit since it would lead to an enhancement at low rapidity and a narrowing of the theoretical spectrum [9].

The clue to a solution lies in the proton rapidity spectrum which seems to indicate that system carries a memory of the direction of the colliding nuclei. The collision can be viewed in the following manner: Two nuclei approach at relativistic speeds, pass through each other and carry on their way, leaving behind a flat, *boost-invariant* central rapidity region of quanta with zero net baryon number. This central region is flowing longitudinally in a Lorentz-invariant way. This model was proposed by Bjorken [11] and explains this anisotropy in terms of longitudinally flowing matter with locally thermalised distributions. Thus the rapidity spectrum is made up of individual thermal sources, each with a different flow angle η:

$$\frac{dN}{dy} = \int_{\eta_{min}}^{\eta_{max}} d\eta \frac{dN_{th}}{dy}(y - \eta) , \tag{2.5}$$

where dN_{th}/dy is given by equation 2.4. Note the restriction on η: There is only a finite amount of energy going into the collision and a large portion of the longitudinal

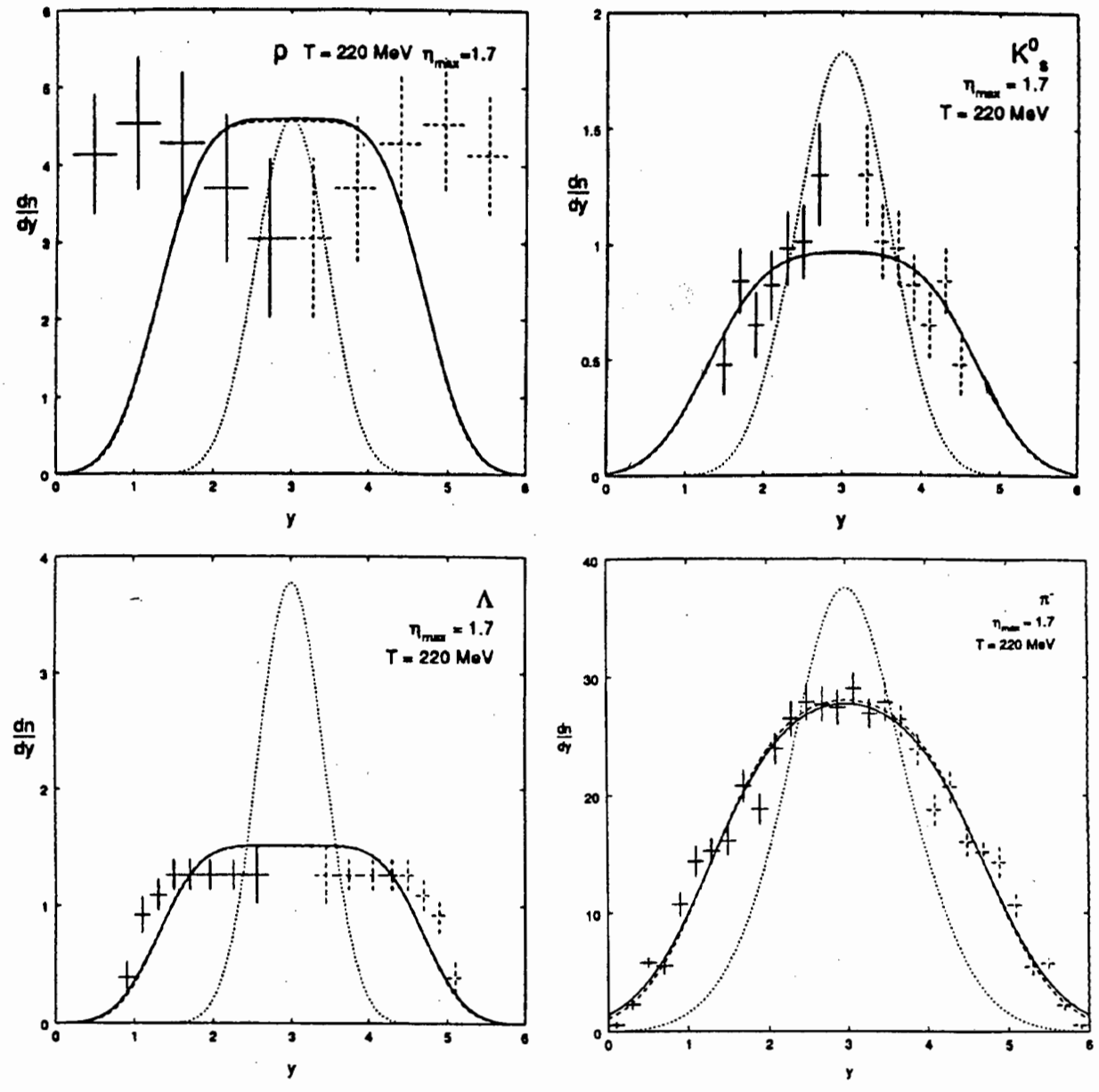

Figure 2.3: Rapidity spectra for various particles from the NA35 S+S experiment. The dotted lines represent the theoretical rapidity curves without any flowing source. The solid lines are the theoretical curves, corrected by considering the spectrum coming from a flowing source [9].

momentum is carried away by the two colliding nuclei. Hence the pion rapidity spectrum tends more towards a Gaussian than a curve with a central plateau. The limits of the integration (η_{min}, η_{max}) are used as a free parameter to fit the pion rapidity spectrum. Keeping the same value for η_{max} seems to fit the other spectra reasonably well, apart from the proton rapidity spectrum which is contaminated by the remnants of the two receding nuclei (see figure 2.3).

2.5.2 Transverse flow

In a "Bjorken" scenario where the incoming ions pass through each other at asymptotically high energies, there is little place for transverse flow. However, as the size of the colliding ions has increased, so has the amount of "stopping" and intuitively one would expect some transverse hydrodynamical flow to result. Evidence indicating greater stopping may be seen in figure 2.4. The rapidity spectrum of protons from NA49 Pb–Pb data tends towards a Gaussian shape with a central plateau rather than the two distinct "humps" seen in the NA35 experiment. Nuclear transparency seems to be greatly reduced and one would expect to see increased transverse flow. Figure 2.5 presents evidence of a strong transverse flow effect in NA44 Pb–Pb data.

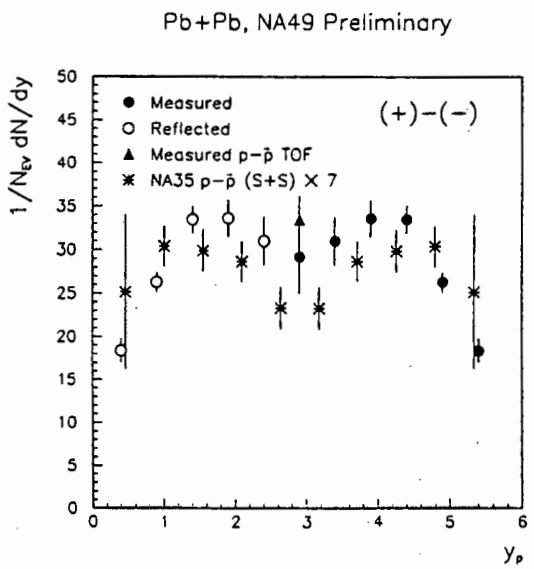

Figure 2.4: Proton rapidity spectrum from NA49 Pb–Pb data (circles and triangle) compared with NA35 S–S data (asterisks). The data has been reflected about $y_p = 3$ and the rapidity spectrum from NA35 has been scaled up by a factor of 7 [37].

We can expect transverse flow to make itself evident in two ways. Firstly, in the flattening of the m_T spectra at high m_T due to the rise in the number of particles with larger m_T. Secondly, in a hydrodynamical picture, all the particles will be flowing with similar velocities. Thus heavier particles will have greater kinetic energy and will appear "hotter". One can therefore expect the slopes of transverse mass plots of the heavier hadrons, to be flatter (since slope $\alpha \; -1/T$)

Figure 2.5 provides a startling illustration of the apparent rise in temperature of the heavier hadrons. The kaon spectrum in particular shows a marked flattening at high m_T. Dashed lines of the form

$$\frac{dN}{m_T dm_T} = C \cdot \exp\left(-\frac{m_T}{T}\right)$$

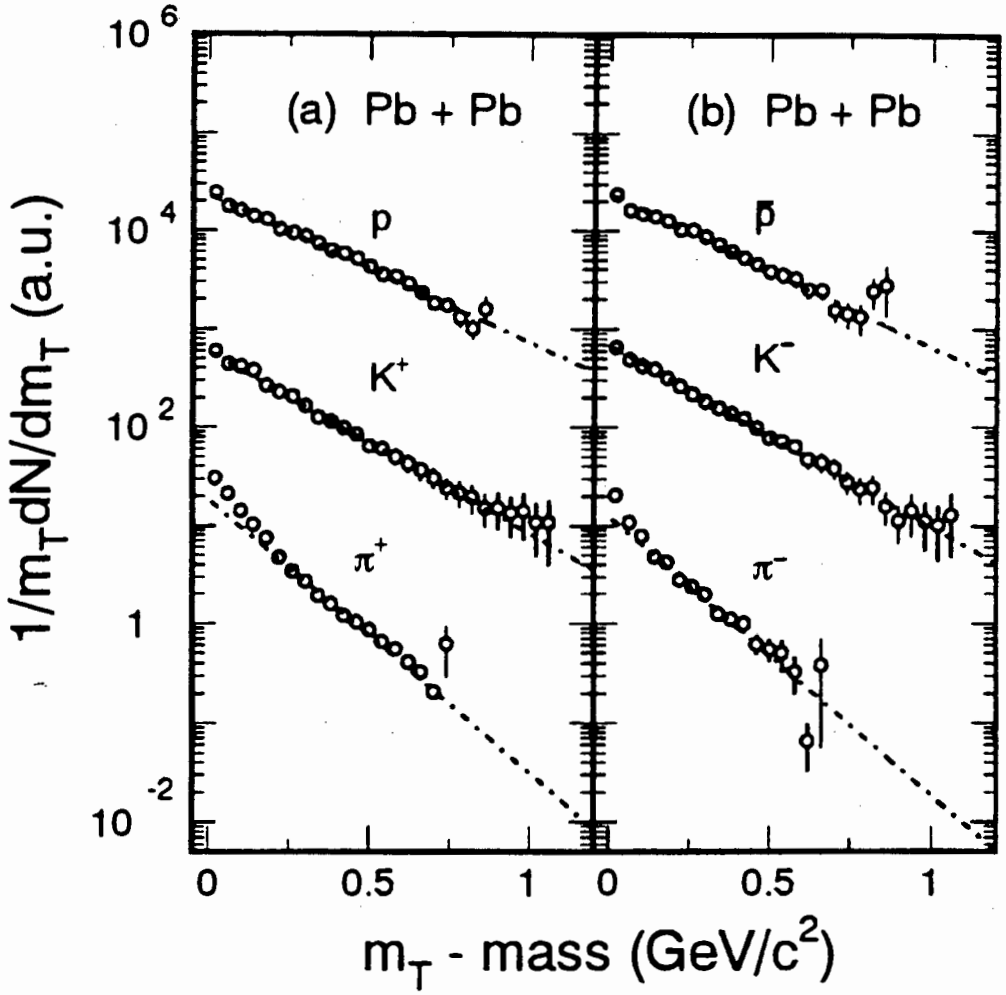

Figure 2.5: Transverse mass distributions from NA44 Pb–Pb collisions with exponential fits [24]. Note the marked difference between the gradients of the pion, kaon and proton spectra. Observe also the flattening of the kaon spectrum at high m_T; one would expect strange particles to be good indicators of flow.

were fitted to the spectra in figure 2.5, with T the obvious parameter determining the gradient of the slope on a semi-log plot. The following table presents the best fit temperatures (in MeV) for all the spectra in figure 2.5 [24].

π^+	K^+	p	π^-	K^-	$\bar{p}$
156 ± 6	234 ± 6	289 ± 7	154 ± 8	235 ± 7	278 ± 9

Table 2.1: This table presents the best fit temperatures (in MeV) to the various transverse mass spectra in figure 2.5. The "apparent" temperatures of the various hadrons do not agree within acceptable experimental uncertainty and provide an indication of transverse flow.

Flow in general and transverse flow in particular, will be covered in more detail in chapter 3.

2.6 Conclusion

Although the formulation of the hadron gas model and the inclusion of hydrodynamical flow is far from complete, it is safe to comment (without spoiling any surprises) that the model has met with considerable success. A stationary thermal model with the inclusion of longitudinal flow can explain most particle spectra reasonably well, with the proton dN/dy spectrum being explained in terms of nuclear transparency. Subsequent chapters will cover the inclusion of transverse flow and resonance decays into the picture, in an attempt to fit the apparent rise in temperature of the heavier particles and the low m_T anomaly in the pion transverse mass spectrum.

In the light of the success of a statistical approach, there is a strong case to be made for thermalisation after the collision has taken place. It is indeed surprising that such a small system can be explained by statistics at all. It seems to run counter to intuition that such a small number of particles can undergo enough collisions in such a small time frame to appear thermalised and (possibly) chemically equilibrated.

Weisskopf was probably the first to observe the possibility that a small, strongly interacting system (such as a compound excited nucleus) could be described in a statistical manner [34]. What is it about the nature of the strong force that allows us to do this? It was the possibility of applying statistics to small, strongly interacting systems and many other observations which lead Hagedorn to propose the statistical bootstrap model which contained an exponentially growing mass spectrum and a critical temperature [33]. This critical temperature basically meant that a gas of hadrons could not be heated up beyond a certain temperature. Instead the system would respond to an excess of energy by simply producing more particles. This critical temperature is interpretted as the temperature at which a phase transition should occur. But where is a QGP hiding in all of this? The gas of hadrons into which the QGP decays cannot retain a memory of its initial state (in which a QGP may have existed) since it must decay into the hadron gas with a maximum allowed temperature. We are only observing a statistical gas at freeze-out. There is no apparent way of telling what was going on before this. If, for example, we can accurately determine the freeze-out temperature with our model, we still do not know whether we ever reached sufficient temperature and energy density to create a QGP.

Why then do we use a hadron gas model? We can only apply it to the study of heavy ion collisions in an attempt to understand and model the dynamics of the system, understand its collective motion (if there is any), and calculate observables such as the temperature. The aim is to understand why statistics works on a dense, strongly interacting system. By attempting to understand the system statistically we can only hope that some secrets about the nature of strong interaction may be revealed in answer to these questions.

Chapter 3

Hydrodynamical flow and freeze-out hypersurfaces

In chapter 2 we made a brief incursion into longitudinal and transverse flow as a necessary expansion to a stationary thermalised gas of hadrons. This chapter intends to cover the mathematics of this in more depth and examine transverse flow in closer detail.

3.1 The invariant, single-particle momentum spectrum

In chapter 2 we were able to describe the momentum spectrum very intuitively with a simple Boltzmann formalism:

$$E\frac{d^3N}{d^3p} = \frac{gV}{(2\pi)^3}Ee^{-(E-\mu)/T} .$$

Unfortunately, when the gas is flowing, the energy E and volume V do not remain Lorentz invariant and it no longer makes sense to simply integrate out the volume as has been done above.

To formulate a more generally invariant model, we start by assuming that all the hadrons are in thermal equilibrium until they decouple. (Previously the volume V was the decoupling boundary.) Generally, this will be a space-time freeze-out hypersurface which we will call σ. If $d\sigma_\lambda$ is an element of this surface and f is the phase space distribution function, then the flow of particles crossing the surface is [23]:

$$\int_\sigma d\sigma_\lambda \int \frac{d^3p}{E} P^\lambda f(x,p) ,$$

and the invariant momentum spectrum is given by the Cooper-Frye formula [22],

$$E\frac{d^3N}{dp^3} = \int_\sigma f(x,P)P^\lambda d\sigma_\lambda \,. \tag{3.1}$$

The general invariant distribution function becomes:

$$f(x,p) = (\exp[(U^\nu(x)P_\nu - \mu(x))/T(x)] \pm 1)^{-1} \,,$$

with U describing the collective flow of the gas. Note that by substituting $U^\nu = (1,0,0,0)$ for the case of a stationary fireball, we regain Boltzmann statistics.

The freeze-out hypersurface marks a boundary between collective flow and free streaming. In other words, it marks the point at which the gas ceases to behave as a statistical and hydrodynamical unit, the participating particles cease to interact with each other and stream freely towards the detectors. The particles of the gas carry a memory of the direction in which they were flowing and memory of the momentum spectra of the gas from which they came. By integrating over this hypersurface, we are effectively integrating over the whole space-time history of the flowing fireball rather than over a static volume.

3.2 Spectrum from a flowing source

To include flow into the picture, one can start by considering the fireball as a cylindrical tube of radius R, expanding both longitudinally (in the z direction) and radially or transversely (in the r direction). We start by focussing on the transverse direction and can give the fireball a longitudinal boost at a later stage. We define the transverse velocity field of a slice of the fireball using a radial space-time boost angle

$$\rho = \frac{1}{2}\ln\left(\frac{t+r}{t-r}\right) = \frac{1}{2}\ln\left(\frac{1+\beta(r)}{1-\beta(r)}\right) = \tanh^{-1}\beta(r) \,, \tag{3.2}$$

where

$$\beta(r) = \beta_s\left(\frac{r}{R}\right)^n$$

in the region $0 \le r \le R$. Here β_s is the velocity of the fireball surface at $r = R$. Thus the fireball has a collective transverse velocity field:

$$U^\nu = (\cosh\rho, \vec{e}_r \sinh\rho, 0) = (\cosh\rho, \cos\phi\sinh\rho, \sin\phi\sinh\rho, 0) \,. \tag{3.3}$$

The velocity field can now be boosted longitudinally by a boost angle η to complete the picture:

$$U^\nu = (\cosh\rho\cosh\eta, \vec{e}_r\sinh\rho, \cosh\rho\sinh\eta) \,.$$

Realising that in cylindrical coordinates,

$$P_\nu = (m_T\cosh y, -p_T\cos\varphi, -p_T\sin\varphi, -m_T\sinh y) \,,$$

it follows that

$$U^\nu P_\nu = m_T \cosh(y-\eta)\cosh\rho - p_T\cos(\phi-\varphi)\sinh\rho\ . \tag{3.4}$$

The next task is to find a suitable freeze-out hypersurface. Freeze-out can only be based on a fairly arbitrary criterion. It is the point at which the particles decouple from the gas and stream freely towards the detectors. The freeze-out criterion is based on the attainment of a suitable mean free path or a low enough temperature. It can be shown that freeze-out points may be widely scattered in space-time and thus it is difficult to define a continuous freeze-out hypersurface [25]. Schnedermann, Sollfrank and Heinz [9] choose to parameterise the hypersurface in cylindrical coordinates:

$$\sigma^\lambda(r,\phi,\zeta) = \{t(\zeta), r\cos\phi, r\sin\phi, z(\zeta)\}\ , \tag{3.5}$$

with $0 \le r \le R$, $0 \le \phi \le 2\pi$ and $-\eta_{max} \le \zeta \le \eta_{max}$. Examining equation 3.5 should indicate that the transverse direction has been kept simple, instantaneous freeze-out has been assumed, but the longitudinal direction has been parameterised with the variable ζ so as to allow for more complicated geometry. For instance, Bjorken has demonstrated in his model [11] that the gas starts to freeze out from its centre (hyperbolas in space-time in the longitudinal direction). A normal surface element is given by

$$d\sigma_\lambda = -\varepsilon_{\lambda\nu\mu\rho}\frac{\partial\sigma^\nu}{\partial r}\frac{\partial\sigma^\mu}{\partial\phi}\frac{\partial\sigma^\rho}{\partial\zeta}dr d\phi d\zeta\ ,$$

where $\varepsilon_{0123} = 1$ and is antisymmetric about the interchange of any two indices.

After a little tensor manipulation, one may derive for the choice (3.5):

$$d\sigma_\lambda = \left(\frac{\partial z}{\partial\zeta}, 0, 0, -\frac{\partial t}{\partial\zeta}\right) r dr d\phi d\zeta\ ,$$

and from here it is straightforward to obtain:

$$P^\lambda d\sigma_\lambda = \left(E\frac{\partial z}{\partial\zeta} - p_z\frac{\partial t}{\partial\zeta}\right) r dr d\phi d\zeta\ . \tag{3.6}$$

We can now make the high temperature approximation:

$$E\frac{d^3N}{d^3p} \approx \frac{g}{(2\pi)^3}\int_\sigma \exp\left(\frac{-(U^\nu P_\nu - \mu)}{T}\right) P^\lambda d\sigma_\lambda\ .$$

Substituting in results from 3.4 and 3.6 we get:

$$E\frac{d^3N}{d^3p} = \frac{g}{(2\pi)^3}\Upsilon\int_0^R r dr \exp\left(-\frac{m_T\cosh(y-\eta)\cosh\rho - \mu}{T}\right)\int_0^{2\pi} d\phi \exp\left(\frac{p_T\cos(\phi-\varphi)\sinh\rho}{T}\right)\ ,$$

where

$$\Upsilon(y) = \int_{-\eta_{max}}^{\eta_{max}} d\zeta\left(m_T\cosh y\frac{\partial z}{\partial\zeta} - m_T\sinh y\frac{\partial t}{\partial\zeta}\right)\ .$$

Using the modified Bessel function:

$$I_0(z) = \frac{1}{2\pi}\int_0^{2\pi} e^{z\cos\phi}d\phi\ ,$$

one integral can be solved:

$$\int_0^{2\pi} d\phi \exp\left(\frac{p_T\cos(\phi-\varphi)\sinh\rho}{T}\right) = 2\pi I_0\left(\frac{p_T\sinh\rho}{T}\right)\ .$$

Substituting cylindrical coordinates and integrating out rapidity y,

$$\frac{dN}{m_T dm_T} = \frac{gm_T}{2\pi}e^{\mu/T}\int_{-\eta_{max}}^{\eta_{max}}d\zeta\int_0^R rdr\int_{-\infty}^{\infty}dy\left(\cosh y\frac{\partial z}{\partial\zeta}-\sinh y\frac{\partial t}{\partial\zeta}\right)\exp\left(-\frac{m_T\cosh(y-\eta)\cosh\rho}{T}\right)I_0\left(\frac{p_T\sinh\rho}{T}\right)\ .$$

The rapidity integral can be done with the help of the modified Bessel function $K_1(z) = \int_0^\infty \cosh y e^{-z\cosh y}dy$, and realising that:

$$\int_{-\infty}^{\infty}(A\cosh y - B\sinh y)\,e^{z\cosh(y-\eta)}dy = 2(A\cosh\eta - B\sinh\eta)K_1(z)\ ,$$

one may arrive at the result

$$\frac{dN}{m_T dm_T} = \frac{gm_T}{\pi}e^{\mu/T}\int_{-\eta_{max}}^{\eta_{max}}d\zeta\left(\cosh\eta\frac{\partial z}{\partial\zeta}-\sinh\eta\frac{\partial t}{\partial\zeta}\right)\int_0^R rdrK_1\left(\frac{m_T\cosh\rho}{T}\right)I_0\left(\frac{p_T\sinh\rho}{T}\right)\ . \tag{3.7}$$

The integral over ζ will yield a constant factor which will only affect the normalisation.

So far we have been examining semilog plots of $dN/m_T dm_T$ vs m_T which (as predicted by a thermal model) will have a slope of $-1/T$. To gain a better understanding of the effects of transverse flow, we start by considering the case where the flow has no r dependence and rather takes on a constant value β_t, say. The slope of a semilog plot of 3.7 will be given by

$$\begin{aligned}\frac{d}{dm_T}\ln\left(\frac{dN}{m_T dm_T}\right) &= \frac{d}{dm_T}\ln\left(m_T I_0\left(\frac{p_T\sinh\rho}{T}\right)K_1\left(\frac{m_T\cosh\rho}{T}\right)\right)\\ &= \frac{I_1\left(\frac{p_T\sinh\rho}{T}\right)}{I_0\left(\frac{p_T\sinh\rho}{T}\right)}\frac{m_T}{p_T}\frac{\sinh\rho}{T} - \frac{K_0\left(\frac{m_T\cosh\rho}{T}\right)}{K_1\left(\frac{m_T\cosh\rho}{T}\right)}\frac{\cosh\rho}{T}\ .\end{aligned}$$

In the limiting case of large p_T it is clear that $p_T \to m_T$ and it can be shown that $K_0/K_1 \to 1$ and $I_1/I_0 \to 1$. Thus the slope reduces to a rather simple expression:

$$\lim_{p_T\to\infty}\frac{d}{dm_T}\ln\left(\frac{dN}{m_T dm_T}\right) = \frac{\cosh\rho-\sinh\rho}{T} = \frac{1}{T}\sqrt{\frac{1-\beta_t}{1+\beta_t}}\ .$$

Comparing this with the expected slope for a stationary fireball, namely: $-1/T$, a "blue-shifted" apparent temperature can be identified:

$$T_{app} = T\sqrt{\frac{1+\beta_t}{1-\beta_t}}\ .$$

Clearly, the more pronounced the transverse flow is, the higher the apparent temperature will be. This analysis only considers the situation of isotropic flow for large p_T. In reality, the mass of each species of particle cannot be ignored and thus the heavier particles will appear hotter. Bearden *et. al.* [24] find a qualitative relationship between the apparent temperature of the particles and their mass and transverse flow velocities:

$$T = T_o + m\langle v_T \rangle^2 \ .$$

This empirical relationship fits the data from the NA44 collaboration extremely successfully (see figure 3.1).

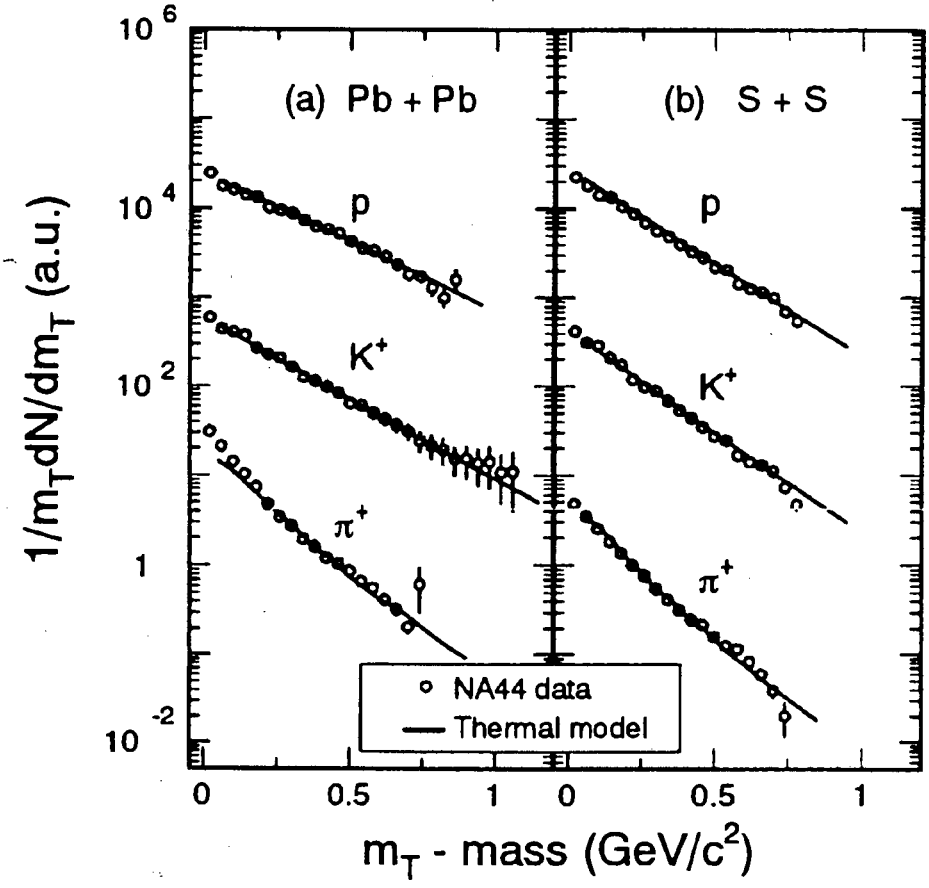

Figure 3.1: A thermal model with transverse flow included, is fitted to the transverse mass spectra from NA44 Pb–Pb collisions at 158 GeV/u (the same data as figure 2.5), and S–S collisions at 200 GeV/u (also from NA44). Resonance decays were included in the pion spectra. The π^+, K^+ and proton spectra from Pb–Pb collisions were fitted with a temperature: $T_o = (140 \pm 7)MeV$ and an average flow: $\langle v_T \rangle = (0.41 \pm 0.11)c$. The spectra from S–S collisions were fitted with a temperature: $T_o = (138 \pm 5)MeV$ and an average flow: $\langle v_T \rangle = (0.28 \pm 0.10)c$ [24].

Chapter 4

The inclusion of resonance decays

Figure 2.1 of chapter 2 demonstrates the incompleteness of the thermal picture that has been built up so far. The decay products of resonances have been ignored, and at the high temperatures of the current experiments, their contribution is significant. A resonance, decaying into a pion and a number of other particles, will have to share out its momentum between all of the decay products. Hence, one would expect to find many pions with low momentum — the presence of resonances in large numbers will shift the momentum spectra of the light particles (pions for example) towards lower momenta, enhancing the yield of pions with low transverse momentum or low longitudinal momentum [1, 3].

4.1 The kinematics of a decaying resonance

Consider a resonance decaying into a pion and n other particles:

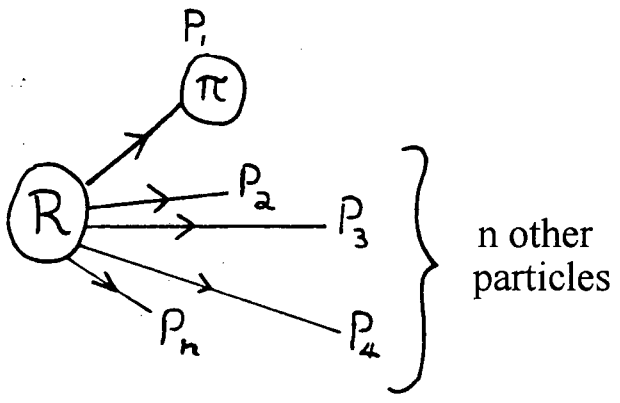

Figure 4.1: A schematic diagram of a resonance decaying into a pion and n other particles.

Applying conservation of energy and momentum in the rest frame of the resonance:

$$P_R^* = P_1^* + P_2^* + \cdots + P_n^*,$$

the following expressions for the energy and the momentum of the pion may be obtained: (see appendix E)

$$E_1^* = \frac{m_R^2 + m_1^2 - W^2}{2m_R},$$

and

$$|\vec{p}_1^*| = \frac{\sqrt{[(m_R + m_1)^2 - W^2][(m_R - m_1)^2 - W^2]}}{2m_R}.$$

Here W is the invariant mass of the other n particles:

$$W = \sqrt{\left(\sum_{i=2}^{n} P_i^*\right)^2},$$

and has the obvious kinematical limits:

$$\left(\sum_{i=2}^{n} m_i\right)^2 \leq W^2 \leq (m_R - m_1)^2 .$$

4.2 A gas of resonances

In obtaining expressions for the spectrum of the pions emitted by decaying resonances in the aftermath of a relativistic heavy ion collision, we begin by assuming that the resonances constitute a thermalised gas [1] and therefore may be described by:

$$N_R = g_R V \int \frac{d^3p_R}{(2\pi)^3} \frac{1}{\exp[\beta(E_R - \mu_R)] \pm 1}, \tag{4.1}$$

where g_R is the degeneracy of the resonance and $\mu_R = B\mu_B + S\mu_S$ is the chemical potential of the resonance coming from its baryon number and strangeness. Converting d^3p_R into cylindrical coordinates: (see appendix C)

$$d^3p_R = 2\pi E m_{TR} dm_{TR} dy_R,$$

and substituting: $E_R = m_{TR}\cosh(y_R)$ (see appendix A), we get:

$$N_R = g_R V \int \frac{dm_{TR}dy_R}{(2\pi)^2} \frac{m_{TR}^2 \cosh(y_R)}{\exp[\beta(m_{TR}\cosh(y_R) - \mu_R] \pm 1}.$$

Finally, realising that we are dealing with extremely high energies, we can make the Boltzmann approximation and end up with:

$$\frac{d^2N_R}{dy_R dm_{TR}} = \frac{g_R V}{(2\pi)^2} \exp(\beta\mu_R) m_{TR}^2 \cosh(y_R) \exp[-\beta m_{TR}\cosh(y_R)]. \tag{4.2}$$

The width of an n particle decay of a resonance in its rest frame is given by the well known formula: [20]

$$\Gamma = \frac{1}{2m_R(2\pi)^{3n-4}} \int \prod_{i=1}^{n} \frac{d^3p_i^*}{2E_i^*} \delta^4\left(P_R^* - \sum_{i=1}^{n} P_i^*\right) \sum_{spins} |\langle f|T|i\rangle|^2 . \tag{4.3}$$

This can now be manipulated by inserting unity [3] in the form:

$$\int_{(\Sigma_{i=2}^{n} m_i)^2}^{(m_R-m_1)^2} dW^2 \delta\left(W^2 - \left(\sum_{i=2}^{n} P_i\right)^2\right) = 1 ,$$

and then splitting up the integral into an effective two body decay (particle 1, a pion or kaon, and the other n particles) and converting to cylindrical coordinates:
$d^3p_1^* = p_{T1}^* dp_{T1}^* d_{L1}^* d\phi^*$, yielding:

$$\Gamma = \frac{1}{2m_R(2\pi)^{3n-4}} \int_{(\Sigma_{i=2}^{n} m_i)^2}^{(m_R-m_1)^2} dW^2 \int_{-|\vec{p}_1^*|}^{|\vec{p}_1^*|} dp_{L1}^* \int_0^{2\pi} d\phi^* g(W^2, p_{L1}^*, \phi^*) ,$$

where:

$$g(W^2, p_{L1}^*, \phi^*) = \int \frac{p_{T1}^* dp_{T1}^*}{2E_1^*} \int \prod_{i=1}^{n} \frac{d^3p_i^*}{2E_i^*} \delta^4\left(P_R^* - \sum_{i=1}^{n} P_i^*\right) \delta\left(W^2 - \left(\sum_{i=2}^{n} P_i\right)^2\right) \sum_{spins} |\langle f|T|i\rangle|^2.$$

Finally, the normalisation is set so that the total decay probability: $\hat{\Gamma}$ is equal to the branching ratio b for a particular decay channel:

$$\hat{\Gamma} = \int_{(\Sigma_{i=2}^{n} m_i)^2}^{(m_R-m_1)^2} dW^2 \int_{-|\vec{p}_1^*|}^{|\vec{p}_1^*|} dp_{L1}^* \int_0^{2\pi} d\phi^* \mathcal{N} g(W^2, p_{L1}^*, \phi^*) = b \tag{4.4}$$

The tools are now in place to perform the calculations necessary to understand how the pions from a gas of decaying resonances occupies the available phase space. Firstly we transform from the rest frame of the resonance to the rest frame of the fireball:

$$\begin{aligned} dp_{L1}^* d\phi^* &= \begin{vmatrix} \frac{\partial \phi^*}{\partial y_1} & \frac{\partial \phi^*}{\partial p_{T1}^2} \\ \frac{\partial p_{L1}^*}{\partial y_1} & \frac{\partial p_{L1}^*}{\partial p_{T1}^2} \end{vmatrix} dy_1 dp_{T1}^2 \\ &= \frac{m_R}{\sqrt{p_{TR}^2 p_{T1}^2 - [E_1^* m_R - m_{T1} m_{TR} \cosh(y_1 - y_R)]^2}} dy_1 dm_{T1}^2 . \end{aligned}$$

Under certain conditions $g(W^2, p_{L1}^*, \phi^*)$ is only a function of W^2 and participating masses and hence Lorentz invariant; Thus:

$$\frac{d^2\hat{\Gamma}}{dy_1 dm_{T1}^2} = \mathcal{N} \int_{(\Sigma_{i=2}^{n} m_i)^2}^{(m_R-m_1)^2} \frac{m_R g(W^2) dW^2}{\sqrt{p_{TR}^2 p_{T1}^2 - [E_1^* m_R - m_{T1} m_{TR} \cosh(y_1 - y_R)]^2}} . \tag{4.5}$$

To get the total particle distribution, we multiply the differential probability 4.5 by $\frac{d^2N_R}{dy_R dm_{TR}}$ and integrate:

$$\frac{d^2N_1}{dy_1 dm_{T1}^2} = \mathcal{N} \int_{(\Sigma_{i=2}^{n} m_i)^2}^{(m_R-m_1)^2} g(W^2) dW^2 \int_{y_R^-}^{y_R^+} dy_R \int_{m_{TR}^-}^{m_{TR}^+} \cdots\cdots \frac{d^2N_R}{dy_R dm_{TR}} . \tag{4.6}$$

Here $m_{TR}^{\pm}$ are the kinematically allowed limits which can be obtained directly from the poles of the Jacobi determinant:

$$m_{TR}^{\pm} = \frac{m_R[E_1^* m_{T1}\cosh(y_1 - y_R) \pm p_{T1}\sqrt{E_1^{*2}p_{T1}^2 - m_{T1}^2\cosh^2(y_1 - y_R)}]}{m_{T1}^2\cosh^2(y_1 - y_R) - p_{T1}^2}\ ; \tag{4.7}$$

the limits: $y_R^- \leq y_R \leq y_R^+$ can now be obtained directly from 4.7 by specifying that $\Delta \geq 0$. This gives:

$$y_R^{\pm} = y_1 \pm \ln\left(\frac{\sqrt{E_1^{*2} + p_{T1}^2} + |\vec{p}_1^*|}{m_{T1}}\right)\ . \tag{4.8}$$

4.2.1 Two-body decays

First, we calculate $g_2(W^2)$ for the case of a two-body decay i.e. a resonance decaying into a pion/kaon and one other particle. Spin effects are neglected and the matrix element is assumed to be constant (and in particular, it is independent of momenta) over the interval being considered. We start with:

$$g_2(W^2) = \frac{|\mathcal{M}|^2}{2}\int\frac{p_{T1}^* dp_{T1}^*}{E_1^*}\int\frac{d^3p_2^*}{2E_2^*}\delta^4(P_R^* - P_1^* - P_2^*)\delta(W^2 - m_2^2)\ .$$

Substituting the identity

$$\int\frac{d^3p_2^*}{2E_2^*} = \int d^4p_2^*\delta(P_2^{*2} - m_2^2)\theta(P_2^{*(0)})\ ,$$

we get:

$$\begin{aligned} g_2(W^2) &= \frac{|\mathcal{M}|^2}{2}\int\frac{p_{T1}^* dp_{T1}^*}{E_1^*}\int d^4p_2^*\delta^4(P_R^* - P_1^* - P_2^*)\delta(P_2^{*2} - m_2^2)\theta(P_2^{*(0)})\delta(W^2 - m_2^2) \\ &= \frac{|\mathcal{M}|^2}{2}\int\frac{p_{T1}^* dp_{T1}^*}{E_1^*}\delta[(P_R^* - P_1^*)^2 - m_2^2]\theta(P_2^{*(0)})\delta(W^2 - m_2^2)\ . \end{aligned}$$

Using: $p_T^2 = E^2 - m^2 - p_L^2 \Rightarrow p_T dp_T = EdE$ and substituting this into $g(W^2)$, we get:

$$\begin{aligned} g_2(W^2) &= \frac{|\mathcal{M}|^2}{2}\int dE_1^*\delta\left(\frac{m_R^2 + m_1^2 - m_2^2}{2m_R} - E_1^*\right)\theta(P_2^{*(0)})\delta(W^2 - m_2^2) \\ &= \mathcal{N}\delta(W^2 - m_2^2)\ . \end{aligned}$$

Here $\mathcal{N}$ is a constant which will be determined by the normalisation:

$$\hat{\Gamma} = \int_{(\Sigma_{i=2}^n m_i)^2}^{(m_R - m_1)^2} dW^2\int_{-|\vec{p}_1^*|}^{|\vec{p}_1^*|} dp_{L1}^*\int_0^{2\pi} d\phi^*\mathcal{N}g_2(W^2) = b$$

$$\Rightarrow \mathcal{N}g_2(W^2) = \frac{b}{4\pi|\vec{p}_1^*|}\delta(W^2 - m_2^2)\ .$$

4.2.2 Three-body decays

In similar fashion to the two-body case, we begin with:

$$g_3(W^2) = \frac{|\mathcal{M}|^2}{2}\int\frac{p^*_{T1}dp^*_{T1}}{E^*_1}\int\frac{d^3p^*_2}{2E^*_2}\int\frac{d^3p^*_3}{2E^*_3}\delta^4(P^*_R - P^*_1 - P^*_2 - P^*_3)\delta(W^2-(P^*_2+P^*_3)^2)\,.$$

Again, the identity:

$$\int\frac{d^3p^*_3}{2E^*_3} = \int d^4p^*_3\delta({P^*_3}^2 - m_3^2)\theta({P^*_3}^{(0)})$$

is substituted and the $\int d^4p^*_3\delta^4(P^*_R - P^*_1 - P^*_2 - P^*_3)$ integration is performed, leaving:

$$g_3(W^2) = \frac{|\mathcal{M}|^2}{2}\int\frac{p^*_{T1}dp^*_{T1}}{E^*_1}\int\frac{d^3p^*_2}{2E^*_2}\delta[(P^*_R - P^*_1 - P^*_2)^2 - m_3^2]\delta(W^2-(P^*_R-P^*_1)^2)\,.$$

Now $d^3p^*_2$ can be converted to spherical coordinates:

$$d^3p^*_2 = |\vec{p}^*_2|E^*_2dE^*_2d(\cos\theta)d\phi\,,$$

using $p^*_2dp^*_2 = E^*_2dE^*_2$. As with the two-body case, we substitute $p_Tdp_T = EdE$ into the first integral. Integrating over ϕ and doing some algebra,

$$g_3(W^2) = \frac{2\pi|\vec{p}^*_2||\mathcal{M}|^2}{8|\vec{p}^*_1||\vec{p}^*_2|}\int dE^*_1\int dE^*_2d(\cos\theta)\delta\left(\frac{W^2+m_2^2-m_3^2+2E^*_2(E^*_1-m_R)}{2|\vec{p}^*_1||\vec{p}^*_2|}-\cos\theta\right)\delta(W^2-(P^*_R-P^*_1)^2)$$

may be obtained. Integrating over $\cos\theta$ and using the limits: $-1 \leq \cos\theta \leq 1$, kinematical limits for E^*_2 may be extracted:

$${E^*_2}^{\pm} = \frac{-(E^*_1-m_R)(W^2+m_2^2-m_3^2) \pm |\vec{p}^*_1|\sqrt{[W^2-(m_2+m_3)^2]\,[W^2-(m_2-m_3)^2]}}{2W^2}\,.$$

Performing the remaining integrals, we arrive at:

$$g_3(W^2) = \left(\frac{\pi|\mathcal{M}|^2}{8m_R}\right)\frac{\sqrt{W^2-(m_2+m_3)^2}\sqrt{W^2-(m_2-m_3)^2}}{W^2}\,;$$

the bracketed term is just a constant which will be determined by normalisation. The normalisation proceeds as before; we start by setting the decay width equal to the branching ratio of the decay:

$$\hat{\Gamma} = \int_{(\Sigma_{i=2}^n m_i)^2}^{(m_R-m_1)^2}dW^2\int_{-|\vec{p}^*_1|}^{|\vec{p}^*_1|}dp^*_{L1}\int_0^{2\pi}d\phi^*\mathcal{N}g_3(W^2) = b\,.$$

The angle ϕ^* and p_{T1} are integrated out and substituting:

$$|\vec{p}^*_1| = \frac{\sqrt{[(m_R+m_1)^2-W^2][(m_R-m_1)^2-W^2]}}{2m_R}\,,$$

we obtain:

$$\frac{2\pi\mathcal{N}}{m_R}\int_{(m_2+m_3)^2}^{(m_R-m_1)^2}dW\frac{\sqrt{(m_R+m_1)^2-W^2}\sqrt{(m_R-m_1)^2-W^2}\sqrt{W^2-(m_2+m_3)^2}\sqrt{W^2-(m_2-m_3)^2}}{W^2} = b\,.$$

Finally, it can be deduced from the equation above that

$$\mathcal{N}g_3(W^2) = \left(\frac{m_R b}{2\pi Q(m_R, m_1, m_2, m_3)}\right)\left(\frac{\sqrt{W^2-(m_2+m_3)^2}\sqrt{W^2-(m_2-m_3)^2}}{W^2}\right), \tag{4.9}$$

with

$$Q(m_R, m_1, m_2, m_3) = \int_c^b \frac{dx}{x}\sqrt{a-x}\sqrt{b-x}\sqrt{x-c}\sqrt{x-d}\,,$$

where $W^2 = x$, $(m_R + m_1)^2 = a$, $(m_R - m_1)^2 = b$, $(m_2 + m_3)^2 = c$ and $(m_2 - m_3)^2 = d$.

$\mathcal{N}g_2(W^2)$ or $\mathcal{N}g_3(W^2)$ may now be substituted into equation 4.6. Substituting $\mathcal{N}g_2(W^2)$ into 4.6 it is easy to integrate immediately over W^2 and we arrive at:

$$\frac{d^2N_1}{dy_1 dm_{T1}^2} = \frac{m_R b}{4\pi|\vec{p}_1^{\,*}|}\int_{y_R^-}^{y_R^+} dy_R \int_{m_{TR}^-}^{m_{TR}^+} \frac{dm_{TR}}{\sqrt{(m_{T1}^2\cosh^2(y_1-y_R)-p_{T1}^2)(m_{TR}^+-m_{TR})(m_{TR}-m_{TR}^-)}}\frac{d^2N_R}{dy_R dm_{TR}}\,. \tag{4.10}$$

Note the factorisation of the denominator using its roots: $m_{TR}^{\pm}$.

Substituting $\mathcal{N}g_3(W^2)$ into 4.6, it is not possible to simplify the expression any further, all three integrals will have to be done numerically as we shall see.

4.3 The transverse momentum spectrum

To find an expression for the transverse momentum spectrum of pions from resonance decays, we begin by integrating out the rapidity. To do this, we introduce a new variable: $\tilde{y}_R = y_R - y_1$ [3]. This causes $d^2N_R/dy_R dm_{TR}$ to be the only part of the integrand which is a function of y_1 and the integration can be done analytically:

$$\begin{aligned}\int_{-\infty}^{\infty} dy_1 \frac{d^2N_R}{dy_R dm_{TR}} &= \frac{g_R V m_{TR}^2 e^{\beta\mu_R}}{4\pi^2}\int_{-\infty}^{\infty}\cosh(\tilde{y}_R+y_1)\exp[-\beta m_{TR}\cosh(\tilde{y}_R+y_1)]dy_1 \\ &= \frac{g_R V}{2\pi^2}e^{\beta\mu_R}m_{TR}^2 K_1\left(\frac{m_{TR}}{T}\right)\,.\end{aligned}$$

Thus:

$$\frac{dN_1}{dm_{T1}^2} = \frac{g_R b V m_R e^{\beta\mu_R}}{8\pi^3|\vec{p}_1^{\,*}|}\int_{\tilde{y}_R^-}^{\tilde{y}_R^+}\int_{m_{TR}^-}^{m_{TR}^+}\frac{m_{TR}^2 K_1\left(\frac{m_{TR}}{T}\right)dm_{TR}}{\sqrt{(m_{T1}^2\cosh^2(y_1-y_R)-p_{T1}^2)(m_{TR}^+-m_{TR})(m_{TR}-m_{TR}^-)}}, \tag{4.11}$$

For the case of two-body decays. The $\tilde{y}_R$ limits are now:

$$\tilde{y}_R^{\pm} = y_R^{\pm} - y_1 = \pm\ln\left(\frac{\sqrt{E_1^{*2}+p_{T1}^2}+|\vec{p}_1^{\,*}|}{m_{T1}}\right)\,.$$

Equation 4.11 must now be integrated numerically, but in order to use Gaussian quadrature we need to make three consecutive variable substitutions [30], First:

$$x = \frac{m_{TR}}{T} \quad , \quad x = \frac{m_{TR}^-}{T} = a \quad , \quad x = \frac{m_{TR}^+}{T} = b \, ,$$

then

$$x = \frac{1}{2}(b-a)y + \frac{1}{2}(b+a) \, ,$$

and finally: $y = \cos\theta$. This leaves us with:

$$\frac{dN_1}{dm_{T1}^2} = \frac{g_R V b T^2 m_R e^{\beta\mu_R}}{32\pi^3|\vec{p}_1^*|} \int_{\tilde{y}_R^-}^{\tilde{y}_R^+} d\tilde{y}_R \int_0^\pi \frac{(b-a)^2\cos^2\theta + 2(b^2-a^2)\cos\theta + (b+a)^2}{\sqrt{m_{T1}^2\cosh^2(\tilde{y}_R) - p_{T1}^2}} K_1\left[\frac{1}{2}((b-a)\cos\theta + a + b)\right] d\theta \, . \tag{4.12}$$

An almost identical process will leave us with a three dimensional integral in the case of a three-body decay.

4.4 The rapidity distribution

To compute the rapidity distribution dN_1/dy_1 of pions produced by decaying resonances, we need to return to equation 4.10 and integrate over m_{T1}:

$$\frac{dN_1}{dy_1} = \frac{m_R b V g_R e^{\beta\mu_R}}{8\pi^3|\vec{p}_1^*|} \int_{y_R^-}^{y_R^+} dy_R \int_{m_{TR}^-}^{m_{TR}^+} dm_{TR} \int_{m_{T1}^-}^{m_{T1}^+} \frac{m_{TR}^2 \cosh y_R \exp[-\beta m_{TR}\cosh y_R] m_{T1} dm_{T1}}{\sqrt{p_{TR}^2 p_{T1}^2 - [E_1^* m_R - m_{T1} m_{TR}\cosh(y_1 - y_R)]^2}} .$$

The denominator of the integrand is quadratic in m_{T1} and so the innermost integral takes on the form:

$$\int \frac{x\,dx}{\sqrt{R}} \, , \qquad \text{where:} \qquad R = ax^2 + bx + c \, . \tag{4.13}$$

Rearranging the denominator of the integrand so that it is a quadratic in m_{T1}, the innermost integral takes on the form:

$$\int_{m_{T1}^-}^{m_{T1}^+} \frac{(m_{TR}^2\cosh(y_R)\exp[-\beta m_{TR}\cosh(y_R)])\, m_{T1} dm_{T1}}{\sqrt{-(m_{TR}^2\sinh^2(y_1 - y_R) + m_R^2)m_{T1}^2 + (2E_1^* m_R m_{TR}\cosh(y_1 - y_R))m_{T1} - (E_1^{*2} m_R^2 + p_{TR}^2 m_1^2)}} \, ,$$

from which one can extract:

$$a = -(m_{TR}^2\sinh^2(y_1 - y_R) + m_R^2) \quad , \quad b = 2E_1^* m_R m_{TR}\cosh(y_1 - y_R) \, ,$$

and

$$c = -(E_1^{*2} m_R^2 + p_{TR}^2 m_1^2) \, .$$

Clearly $a \leq 0$ for all possible values, and we can require $\Delta \geq 0$. Under these conditions the integral has the following solution: [16]

$$\int_{m_{T1}^-}^{m_{T1}^+} \frac{x\,dx}{\sqrt{R}} = \frac{\sqrt{R}}{a}\Bigg|_{m_{T1}^-}^{m_{T1}^+} + \frac{b}{2a\sqrt{-a}} \arcsin\left(\frac{2ax+b}{\sqrt{b^2-4ac}}\right)\Bigg|_{m_{T1}^-}^{m_{T1}^+} , \tag{4.14}$$

where the limits, $m_{T1}^{\pm}$, may be found by specifying: $R \geq 0$. This yields:

$$m_{T1}^{\pm} = \frac{E_1^* m_R m_{TR} \cosh(y_1 - y_R) \pm p_{TR}\sqrt{|\vec{p}_1^*|^2 m_R^2 - m_{TR}^2 m_1^2 \sinh^2(y_1 - y_R)}}{m_{TR}^2 \sinh^2(y_1 - y_R) + m_R^2} ,$$

and as before, by requiring that $\Delta \geq 0$, we can extract the limits for y_R:

$$y_R^{\pm} = y_1 \pm \ln\left(\frac{|\vec{p}_1^*| m_R + \sqrt{|\vec{p}_1^*|^2 m_R^2 + m_{TR}^2 m_1^2}}{m_{TR} m_1}\right) .$$

Substituting a, b, and c into equation 4.14, one may find after a little algebra, that the first term disappears and we are left with:

$$\int_{m_{T1}^-}^{m_{T1}^+} \frac{x dx}{\sqrt{R}} = \frac{-b}{2a\sqrt{-a}}(\arcsin(-1) - \arcsin(1)) = \frac{-b}{2a\sqrt{-a}} \arccos(-1) .$$

Thus

$$\int_{m_{T1}^-}^{m_{T1}^+} \frac{x dx}{\sqrt{R}} = \frac{E_1^* m_R m_{TR} \cosh(y_1 - y_R)}{(m_{TR}^2 \sinh^2(y_1 - y_R) + m_R^2)^{3/2}} \pi ,$$

and finally we can substitute this result to get:

$$\frac{dN_1}{dy_1} = \frac{m_R^2 b V g_R E_1^* e^{\beta\mu_R}}{8\pi^2 |\vec{p}_1^*|} \int_{m_R}^{\infty} dm_{TR} \int_{y_R^-}^{y_R^+} \frac{m_{TR}^3 \cosh(y_R)\cosh(y_1 - y_R)\exp[-\beta m_{TR}\cosh(y_R)] dy_R}{(m_{TR}^2 \sinh^2(y_1 - y_R) + m_R^2)^{3/2}} . \tag{4.15}$$

Equation 4.15 can now be integrated numerically using Gaussian quadrature.

4.5 Conclusion

This chapter has been devoted to developing the theoretical equations for the momentum spectra of the decay products of a gas of resonances. The usefulness of obtaining expressions for the longitudinal and transverse momentum spectra of pions or kaons from resonance decays cannot be overemphasised. Since pions (and perhaps kaons) from resonance sources tend to outweigh thermal pions in a gas of freeze-out hadrons, they will have a significant impact on the momentum spectra and thus their inclusion is essential. Furthermore a new path of investigation is opened up. The width of the rapidity window chosen by an experimenter will have a significant effect on all the particle ratios. Using the theoretical expressions for dN/dy spectra from thermal and resonance sources, the width of the rapidity window can be chosen in accordance with that used in a particular experiment and a better K/π ratio may be predicted. Using pions and kaons from thermal and resonance sources, one can now predict how the K/π ratio varies with the width of rapidity window.

Chapter 5 will deal with the excess of soft pions in the pion m_T spectrum. Pions from resonance decays will be included in the spectrum in an attempt to fit the data. Chapter 6 will deal with the rapidity spectra of pions and kaons from thermal and resonance sources and use the equations that have been developed to find out how the K/π ratio is affected by the width of the rapidity window used in a particular experiment.

Chapter 5

The low m_T anomaly in the pion momentum spectrum, experiment vs theory

Much has been written about the anomalously large number of pions with low transverse momentum which emanate from a heavy ion collisions. Enhanced production of soft pions can be explained by the presence of large numbers of resonances which decay into pions and other particles. The momentum of the resonance is shared out among the decay products and hence the pion spectrum from resonances will be shifted towards low m_T [1, 3, 4, 5]. The anomalous number of soft pions can also be explained by supposing that they emanate from two sources of markedly differing temperature [26, 27]. The simplest way to solve the problem, however, is to invoke a pion chemical potential: μ_π [28], supposing that the pions are out of chemical equilibrium.

5.1 Do resonance decays explain the low m_T anomaly?

In chapter 4 we developed the tools necessary to draw a more complete picture of the goings on inside a statistical gas of hadrons. Using the particle data table (appendix F) and a computer (to integrate equation 4.12 or its three-body decay equivalent) the pion transverse mass spectrum from each resonance decay can now be calculated. The spectra can then be summed together with direct thermal pions to complete the picture. Although this has been done before [1, 3], to the best of my knowledge, no-one has made up a full particle data table of resonance decays and tried to fit the experimental data with such a complete analysis. Figure 5.1 shows an attempt to fit the π^+ transverse mass spectrum from NA44 data. The theoretical curve includes a complete spectrum of pions from two and three-body resonance decays.

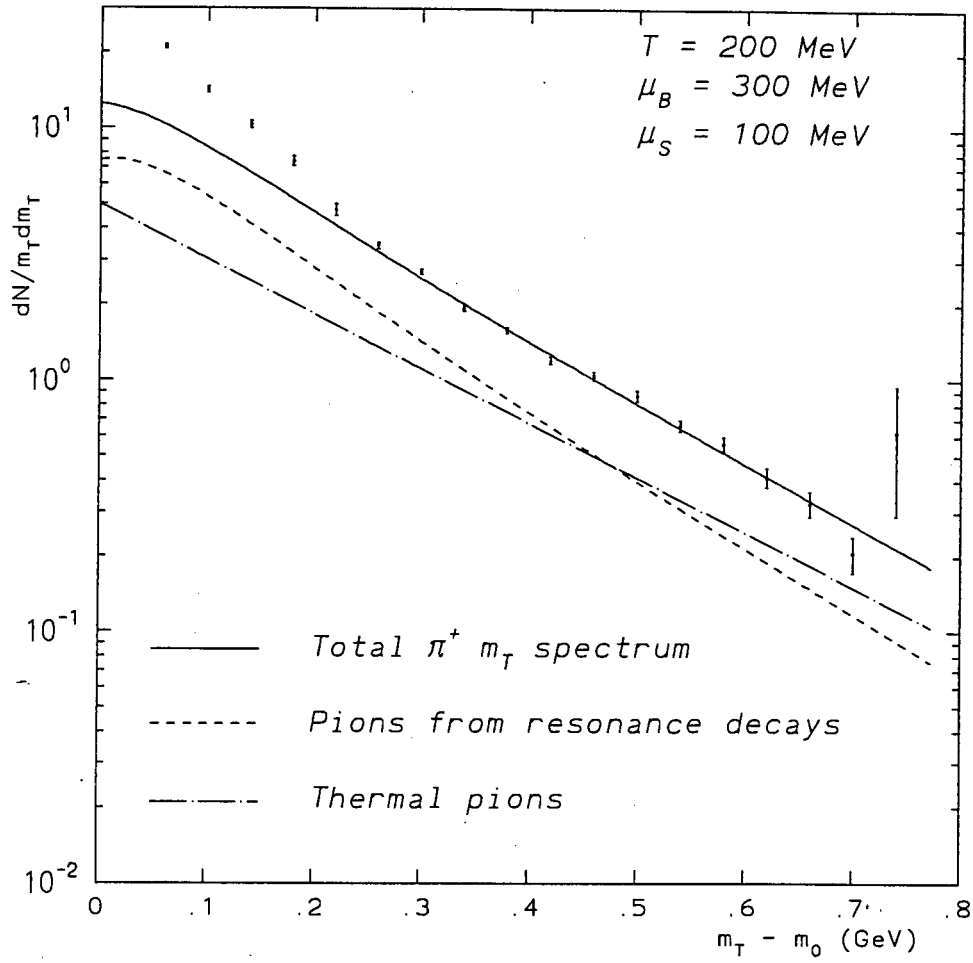

Figure 5.1: A theoretical thermal pion m_T spectrum is fitted to the π^+ transverse mass spectrum from NA44 Pb–Pb data. The theoretical curve includes pions of thermal origin and pions from resonance decays. Possible collective flow effects have been ignored.

Compare figure 5.1 with a similar fit to the π^- transverse mass spectrum from NA35 S+S at 200GeV (figure 5.2). Sollfrank, Koch and Heinz [3] were able to produce an excellent fit, including contributions to the π^- m_T spectrum from only a few key resonances. The inclusion of resonances fits the NA35 data because the low m_T anomaly is not nearly as pronounced as in the NA44 Pb–Pb data. Clearly there must be another mechanism involved in the enhancment of soft pions and curiously, it has only come to the fore in the latest Pb–Pb experiments at CERN. Figure 5.1 demonstrates that the inclusion of resonance decays has failed to explain the low m_T anomaly and other explanations must be sought.

The formulation of a resonance gas to explain the low m_T anomaly has a number of problems associated with it.

- Currently, there is a lack of quality data about the decay channels of the heavier resonances, $m \gtrsim 2\,GeV$. As we raise the temperature of the hadron gas, so heavier

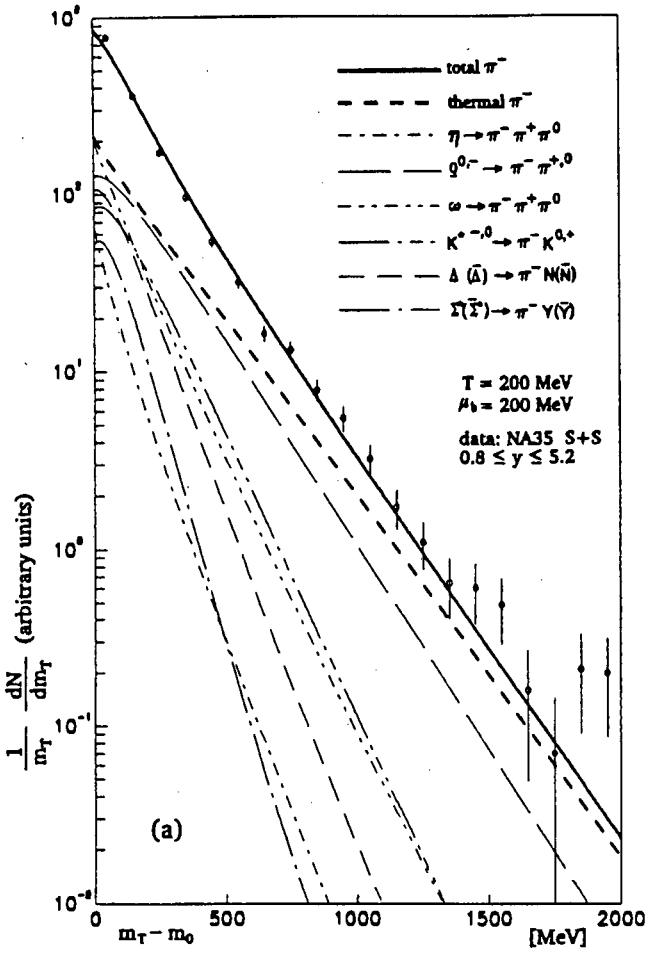

Figure 5.2: The π^- transverse mass spectrum from the NA35 data. The data is fitted with a theoretical curve of direct thermal pions together with pions emanating from a limited number of important resonance decays [3].

resonances are produced in large numbers. At 200 MeV, I determined that the heavy resonances make less than 1% contribution to the pion spectrum. At this temperature, one can still be fairly confident of the model. Resonance production is highly temperature sensitive and formulating a model with any temperature above about 220 MeV would significantly raise their contribution, with the validity of the hadron gas model itself being questionable.

- The problem of successive generations of resonances has been ignored. A heavy resonance will decay into a pion and a lighter (second generation) resonance which will perhaps decay into more pions with even lower momentum. Thus the resonance gas passes through several generations before the final decay products reach the detectors. Pions arising from second and even third generation resonance gases will have a transverse mass spectrum strongly shifted towards low m_T, but whether their contribution to the overall spectrum would be significant is questionable. This

idea must still be tested against the data. Second generation pions have not been included since the calculations look prohibitively complicated. The difficulty of each subsequent analysis, with diminishing returns and exponentially increasing complexity, seems to suggest the need for a fresh approach.

- Many approximations have been made. In particular, we need to consider the possibility that Bose statistics will play a significant role in the enhanced production of soft pions. Perhaps so many approximations have been made, that we have created the anomaly ourselves.

There is no doubt, however, that resonance decays make a significant contribution to the pion spectra and the tools developed in chapter 4 have many useful applications, one of which will be examined in chapter 6.

5.2 Pions from two distinct thermal sources

Sinyukov, Averchenkov and Lörstad [26] suggest that, in the aftermath of a heavy-ion collision, there exist two thermal sources which radiate pions. The hot source is a mixed quark-gluon-hadron phase (which may have contained a QGP "droplet"). The edges of the system, which are less involved in the collision, form a low temperature source of pions. The authors use a two-temperature hydrodynamical model with boost-invariant flow in the longitudinal direction. Figure 5.3 illustrates the success of this approach.

5.3 Are the pions out of chemical equilibrium?

Kataja and Ruuskanen [28] suggest that the pions are strongly out of chemical equilibrium at freeze-out and introduce a positive pion chemical potential, $\mu_\pi \approx 120\,MeV$. Introducing this chemical potential gives the pion transverse mass spectrum a marked concave curvature at low m_T and fits the data remarkably well. It is not clear, however, *why* the pions are out of chemical equilibrium. The authors suggest that as the gas of hadrons cools towards freeze-out, the amount of phase space available to the pions shrinks at a faster rate than the processes which will change the number of pions. Considering the pions' predisposition to interact while in the gas, this hardly seems a likely possibility. Indeed, it seems quite clear that the pions are out of chemical equilibrium, but what this means physically is not apparent.

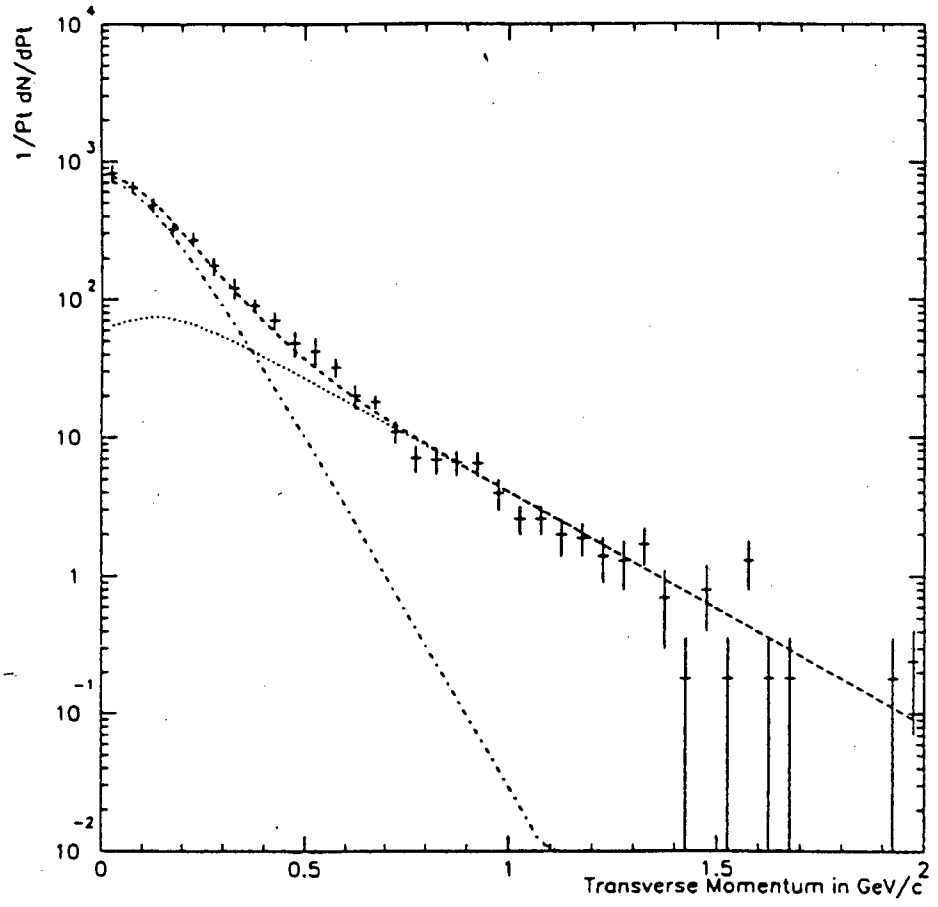

Figure 5.3: The π^- transverse momentum spectrum from NA35 S+S collisions at 200 GeV/u. The data is fitted with a two-component model with temperatures $T_1 = 200\,MeV$ and $T_2 = 80\,MeV$ [26].

5.4 Conclusion

It is apparent that a static model is not going to be sufficient to explain the momentum spectrum of the pions. The success of using a two-temperature thermal model and introducing a pion chemical potential point us in the direction of a more dynamical approach. Shuryak, in trying to explain the "soft photon puzzle" [29], suggests that pions will tend to be reflected at the boundaries of the gas. Combining this with the fact that pions have a mean free path much shorter than the size or lifetime of the collision system, suggests that the pions will freeze out later than other particles. Other particles are able to leave the collision system much earlier because of a lower interaction cross-section, correspondingly the pions will appear cooler than other particles [36].

The problem is now to perform the necessary calculations to decide when the pions are likely to freeze out and find a suitable freeze-out hypersurface. Having performed these calculations, there should be little problem in understanding why there are so many soft pions. Formulated in this way, the puzzle is not so much with the enhanced production

of *low* m_T pions, but rather with the large number of *high* m_T pions. The high m_T anomaly in the pion transverse mass spectrum is, however, decidedly easier to explain. The inclusion of transverse flow (perhaps a superposition of fireballs as opposed to two distinct thermal sources), combined with a finite probability that a "hot" pion could escape from the gas before freeze-out, could be sufficient to complete the picture of pion dynamics. (It is perhaps worth observing successive experiments to see whether there is a correlation between increased transverse flow and increased concavity of the pion transverse mass spectrum.)

If these ideas fail to explain the anomaly, we must consider the possibility of new physics emerging. Because of their interaction, pions could perhaps yield clues about the nature of the strong force and could, in fact, be seen as a useful probe in heavy ion collisions.

Chapter 6

The K/π ratio: The effects of the rapidity window

Particle ratios are nice to predict theoretically since they are unencumbered by free parameters such as the volume of the system, and can assist in the determination of other free parameters (chemical potentials for example). Normally, when calculating particle ratios, we integrate out the rapidity from $-\infty$ to ∞. The experimental picture is however quite different. Experimentalists often use a very small rapidity window of observation and this means that a significant number of particles with large rapidity are neglected. The width of rapidity window chosen will have a significant influence on the experimentally measured particle ratios and our theoretical predictions must be adjusted accordingly.

6.1 Rapidity spectra

To start with, I have plotted the rapidity spectra of pions and kaons from direct thermal sources and from resonance decays. This was done using equation 2.4 (the stationary thermal spectrum) and equation 4.15 (the rapidity spectrum from resonance decays) for each of the various particles ($\pi^{\pm}$, K^{+} and K^{-}).

Referring to figure 6.1, it is noticeable how much more strongly peaked the pion rapidity spectrum from resonance decays is, compared with the direct thermal spectrum. Also noticeable is that the kaon rapidity spectra are much narrower than the pion rapidity spectrum. Longitudinal flow has not been included since various experiments show markedly differing amounts of stopping (compare NA35 data (figure 2.3) with NA49 data (figure 2.4) for instance). Comparing the widths of the $K^{\pm}$ rapidity spectra with the width of the pion rapidity spectrum, one can perhaps already predict how the particle ratios are going to vary with the width of the chosen rapidity window, but it is best to

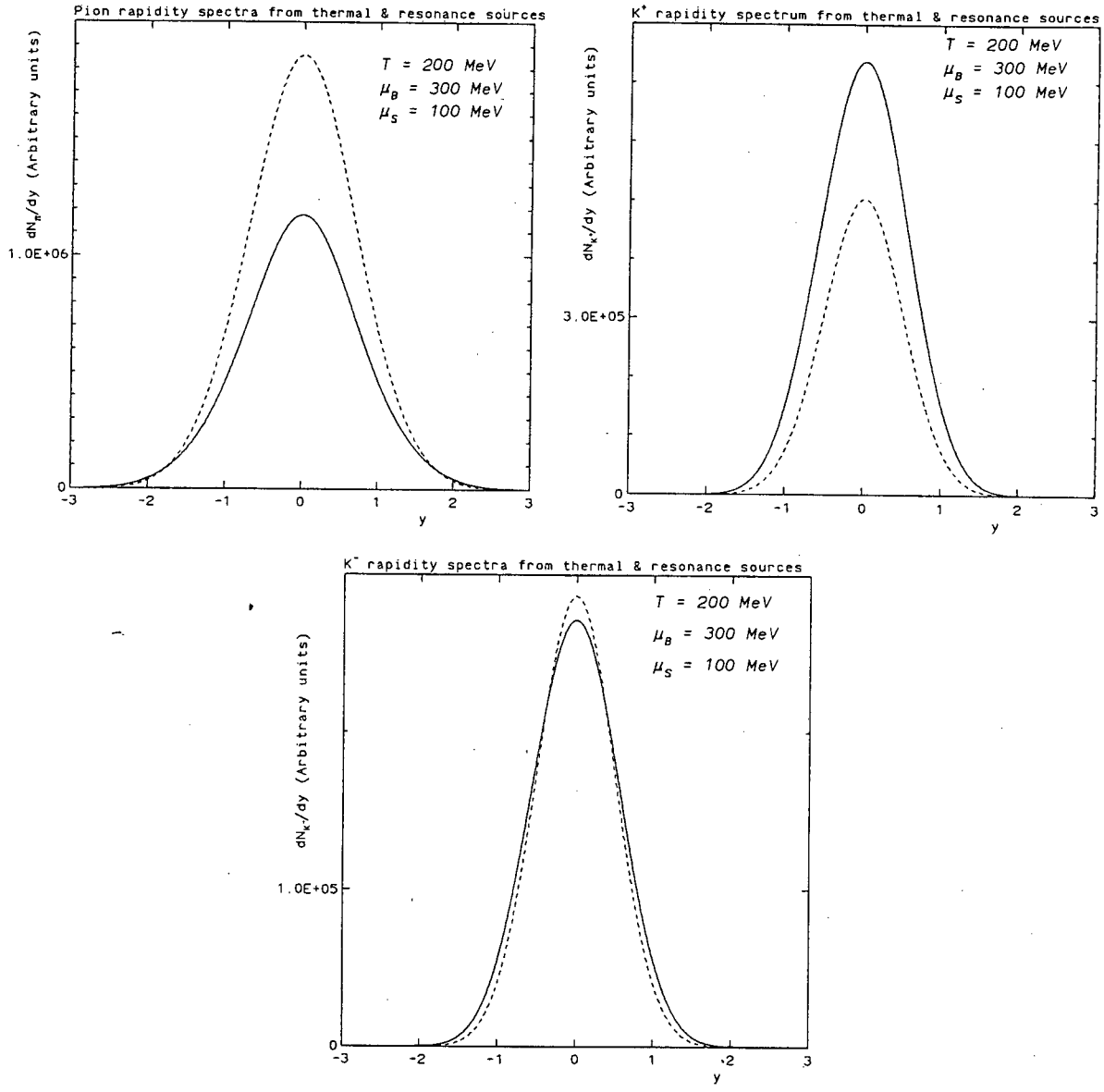

Figure 6.1: Rapidity spectra of pions and kaons from direct thermal sources (solid lines) and resonance decays (dashed lines). A stationary thermal model without transverse flow was used.

actually see some plots to gain some physical insight into what is going on.

6.2 Particle ratios

Figure 6.2 illustrates a similar trend for both the thermal and resonance pictures (the ratio from resonance decays is perhaps a little sharper, but this is to be expected in the light of the enhancement of pions and kaons with low rapidity). It is clear that the K^+/π ratio is maximal for very small rapidity windows and minimal as the width of the window becomes large. By superimposing the K^+ and pion rapidity spectra and moving two

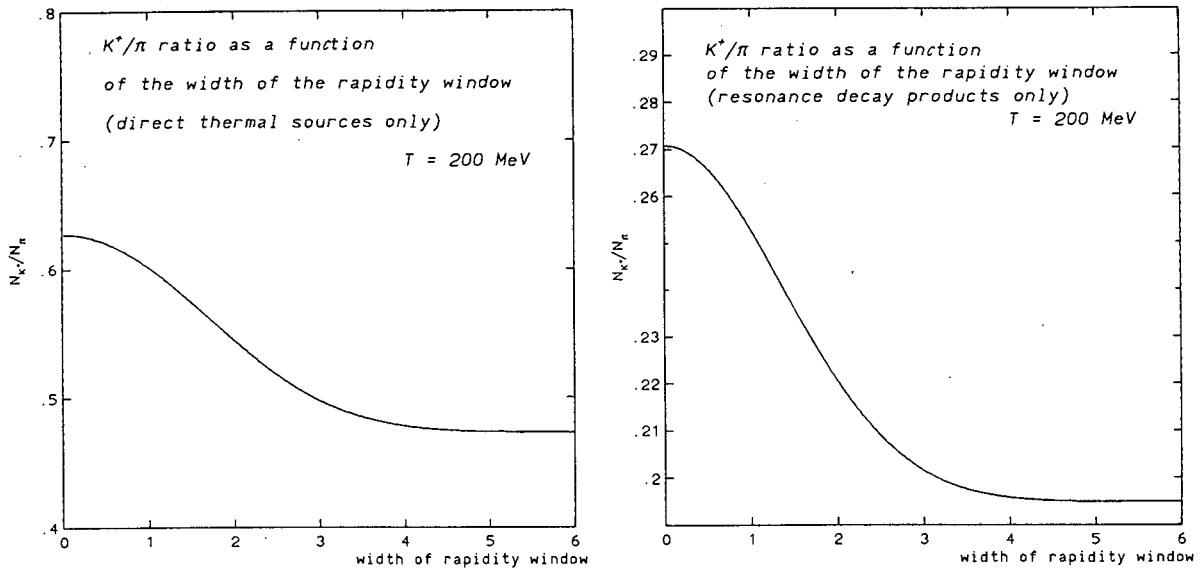

Figure 6.2: The K^+ to π ratio as a function of the width of the rapidity window. The left hand plot uses only a thermal model while the right hand plot includes only decay products of a resonance gas. Chemical potentials: $\mu_B = 300MeV$ and $\mu_S = 100MeV$.

imaginary lines outwards from the centre of the plot (y = 0), one can see that the K^+ spectrum drops off more quickly than the pion spectrum. Thus we can explain the drop in the ratio as the window widens. As one moves further away from the middle, most of the high rapidity pions are gathered into the window and the ratio levels off at some lower value.

Figure 6.3 shows the three basic particle ratios (K^+/π, K^-/π and K^+/K^-) we can calculate with the combined thermal and resonance gas model.

It would be helpful to compare these theoretical curves with various experiments. The application is, however, restricted to experiments with colliding ions of identical mass. In addition, some experiments do not use a symmetrical rapidity window. In principle, however, the calculations can be adjusted to suit a particular experiment with ease.

There are a couple of problems which must be overcome before this analysis is of practical use:

1. Longitudinal flow needs to be included into the picture for a more realistic prediction of the variation of the particle ratios. Each experiment exhibits a different amount of flow, because they use different beams, and thus it is not possible to use these results without further analysis.

2. The particle ratios are particularly sensitive to the choice of chemical potentials. Only when the chemical potentials are established, can this analysis proceed. On the other hand, the tools developed may be useful in determining the chemical

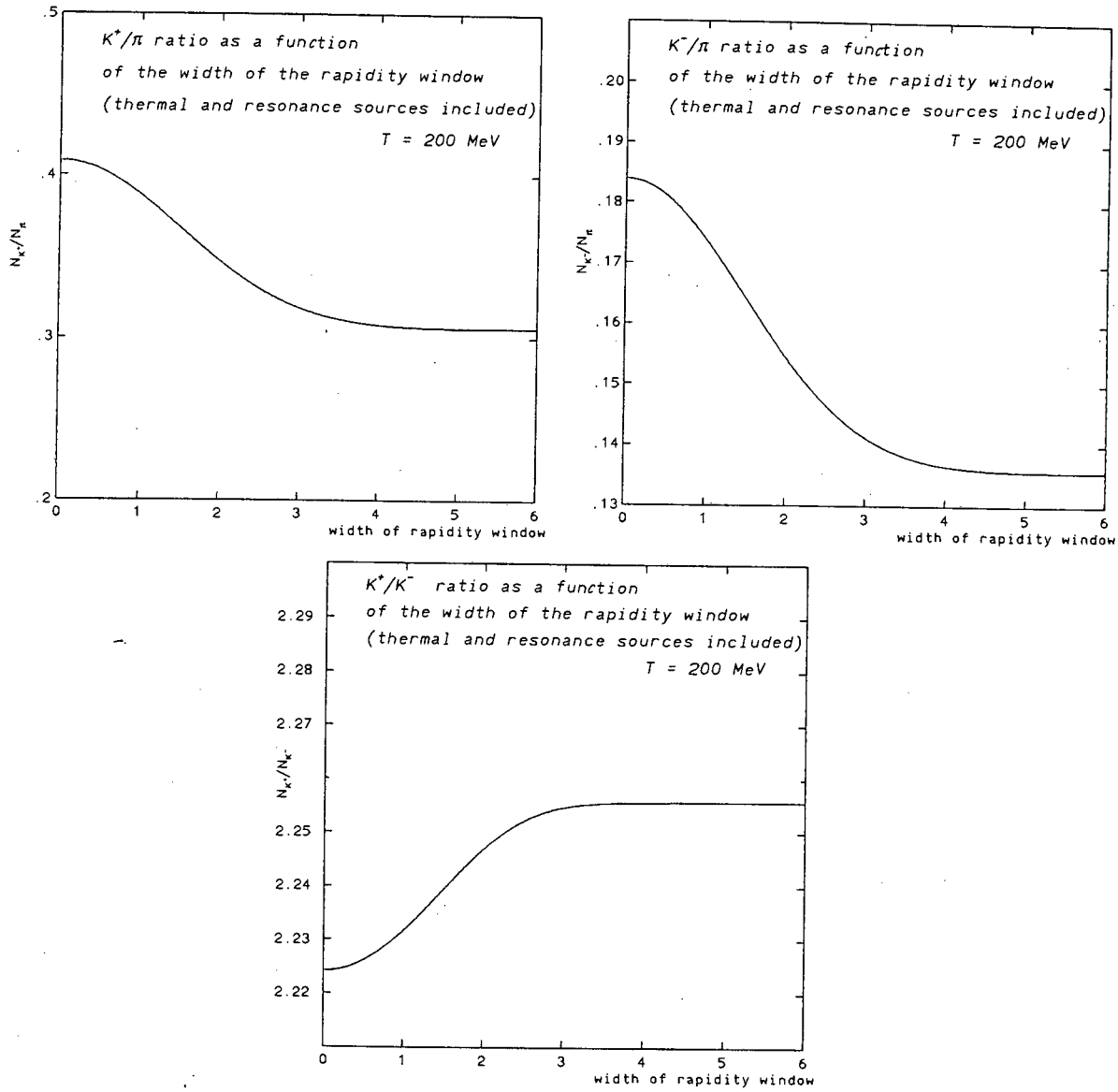

Figure 6.3: Particle ratios as a function of the width of the rapidity window chosen. Chemical potentials are as before, $\mu_B = 300MeV$ and $\mu_S = 100MeV$.

potential of the system via the study of the particle ratios.

Comparing figure 6.2 and figure 6.3 it is noticeable that the inclusion of resonance decays in the calculation of the particle ratios has a significant effect on their values. Secondly, the particle ratios are clearly sensitive to the choice of the rapidity window. It is essential therefore, for experiments with sufficiently high energy and rapidity window less than 4, that resonance decays and the width of the rapidity window are taken into account when comparing experimental particle ratios with theoretically predicted values.

Chapter 7

Conclusion

This thesis began by considering a static Hadron Gas model which was then extended to include transverse flow and resonance decays. Because of the large size of the system, the choice of formalism was Grand Canonical. We have seen that the extended Hadron Gas model has been quite successful in fitting various experimental momentum spectra. The inclusion of resonance decays has, however, failed to explain the low pion m_T anomaly in the latest experimental data. We argue the need for a more dynamical approach to the problem, considering the possibility that the pions are colder than we have predicted due to a later freeze-out time. This idea and the inclusion of transverse flow may be able to explain the marked concavity of the pion transverse momentum spectrum. This is still an area which must be investigated in a great more detail as it may yield new physics.

In chapter 6 we used a combination of thermal sources and resonance decays to examine how the width of the rapidity window and the inclusion of resonance decays affects various particle ratios. The inclusion of resonance decays has been shown to have a significant effect on the particle ratios. In addition, variations in the width of the rapidity window have been shown to affect the particle ratios and therefore the analysis developed in this chapter is essential to any improved understanding of the particle ratios. The tools developed in chapter 6 may be used to improve our prediction of many macroscopic quantities of the heavy ion collision system.

The conclusion to chapter 2 has already discussed some of the problems which face the QGP field. There are specific signatures which will tell us whether a QGP was formed and the evidence of QGP formation in the latest data from the CERN-SPS experiments is mounting. Signals of J/Ψ suppression and enhanced photon and dilepton production are becoming clearer and more convincing. By the time the BNL-RHIC experiments have been completed and analysed, there will probably be little doubt in our minds that a QGP was formed. The realisation that QCD is (at least in part) correct will indicate that the theorists are on the right track, but we need to go further than this.

Macroscopic models such as the Hadron Gas model may be used as a tool to enhance our understanding of how the system behaves and why it behaves the way it does. It will probably never directly tell us whether a QGP was formed, but this is not its intended purpose. Our search is not only for a QGP, but as collision energies increase, we need to try and extract secrets about the nature of the strong interaction. We have a smoking gun, but the bullet needs to be found. This is where a Hadron Gas formalism may play a significant role. As our understanding of the statistical nature of the system increases, hopefully some new physics will be discovered. The strong force has been particularly difficult to understand because it hides inside colour neutral particles. There has been, as a result, a great deal of theoretical speculation about the force without enough experimental data to back it up. If QGP is formed, it will mean that much of the theoretical speculation is indeed correct, but it is up to new experiments to drive the investigation forward and point the theorists in the direction of new physics. We need to answer questions as to why statistics works so well and examine anomalies and discrepancies more closely. Therein lies the future of this field of study.

Appendix A

Kinematic variables and some QGP jargon

A.1 Momentum coordinates

The momentum space coordinates in ultra-relativistic heavy ion collisions are cylindrical. They are chosen this way to suit the nature of the system. The direction of the two incoming nuclei define a unique axis which is referred to as the longitudinal axis or z axis. The plane perpendicular to the z axis is referred to as the transverse direction. The momentum coordinates are thus the longitudinal momemtum, p_z and and the transverse momentum, $p_T = \sqrt{p_x^2 + p_y^2}$.

These momentum coordinates are manipulated a step further into variables which are of more practical use. The transverse mass is defined as

$$m_T = \sqrt{m_0^2 + p_T^2} = \sqrt{m_0^2 + p_x^2 + p_y^2}$$

and the rapidity as:

$$y = \frac{1}{2} \ln \left(\frac{E + p_z}{E - p_z} \right) ,$$

The rapidity expression can be manipulated in the following way:

$$y = \frac{1}{2} \ln \left[\left(\frac{E + p_z}{E - p_z} \right) \left(\frac{E + p_z}{E + p_z} \right) \right] = \ln \left(\frac{E + p_z}{m_T} \right) .$$

Thus

$$e^y = \frac{E + p_z}{m_T} , \tag{A.1}$$

and

$$e^{-y} = \frac{m_T}{E + p_z} . \tag{A.2}$$

Using equations A.1 and A.2 it is straightforward to obtain:

$$\sinh y = \frac{1}{2}\left(e^{y} - e^{-y}\right) = \frac{p_z}{m_T} \Longrightarrow p_z = m_T \sinh y \ ,$$

and

$$\cosh y = \frac{1}{2}\left(e^{y} + e^{-y}\right) = \frac{E}{m_T} \Longrightarrow E = m_T \cosh y \ .$$

Using the definition of $\tanh y$ one can see that

$$\tanh y = \frac{p_z}{E} \ .$$

This will hopefully give an intuitive feel for what rapidity is physically.

A.1.1 Properties of rapidity

Rapidity is a useful variable in that one simply adds rapidities in moving from one inertial frame to another. Consider a particle moving in the lab frame and the centre of mass frame of the collision. If the total energy in the CM frame is $\sqrt{s}$ then the energy and longitudinal momentum are $\gamma_c\sqrt{s}$ and $\beta_c\gamma_c\sqrt{s}$ respectively. The rapidity of the CM frame in the lab frame is thus:

$$y_{cm} = \frac{1}{2}\ln\left(\frac{\gamma_c\sqrt{s} + \beta_c\gamma_c\sqrt{s}}{\gamma_c\sqrt{s} - \beta_c\gamma_c\sqrt{s}}\right) = \frac{1}{2}\ln\left(\frac{1+\beta_c}{1-\beta_c}\right) \ .$$

Now consider the rapidities of our particle in the lab frame and the CM frame (denoted by a $*$)

$$y = \frac{1}{2}\ln\left(\frac{E+p_z}{E-p_z}\right), \quad \text{and} \quad y^* = \frac{1}{2}\ln\left(\frac{E^*+p_z^*}{E^*-p_z^*}\right) \ .$$

Transforming between the frames:

$$\begin{aligned} y = & \ \frac{1}{2}\ln\left(\frac{\gamma_c(E^* + \beta_c p_z^*) + \gamma_c(\beta_c E^* + p_z^*)}{\gamma_c(E^* + \beta_c p_z^*) - \gamma_c(\beta_c E^* + p_z^*)}\right) \\ = & \ \frac{1}{2}\ln\left(\frac{E^*+p_z^*}{E^*-p_z^*}\right) + \ln\left(\frac{1+\beta_c}{1-\beta_c}\right) \\ & \text{that is :} \quad y = y^* + y_{cm} \ . \end{aligned}$$

We can see that the rapidity of a particle in the lab frame is equal to the sum of the rapidity of the particle in the CM frame and the rapidity of the CM frame in the lab frame. Most importantly, the *shape* of the rapidity spectra will be invariant under a Lorentz transformation, everything is just moved along by an amount y_{cm} [35]!

A.1.2 Pseudorapidity

Examining the high energy limit of the rapidity definition will yield another useful variable, namely the pseudorapidity (sometimes denoted by an η). Assume a particle is emitted at an angle θ to the z axis. The rapidity may be written:

$$y = \frac{1}{2}\ln\left(\frac{E+p_z}{E-p_z}\right) = \frac{1}{2}\ln\left(\frac{\sqrt{m_0^2+p^2}+p\cos\theta}{\sqrt{m_0^2+p^2}-p\cos\theta}\right) .$$

For $p \gg m$,

$$y \approx \frac{1}{2}\ln\left(\frac{p+p\cos\theta}{p-p\cos\theta}\right) = \frac{1}{2}\ln\left(\frac{2\cos^2\frac{\theta}{2}}{2\sin^2\frac{\theta}{2}}\right) = -\ln\left(\tan\frac{\theta}{2}\right) .$$

Thus we can define the pseudorapidity:

$$y \approx \eta = -\ln\left(\tan\frac{\theta}{2}\right) .$$

This is a very useful variable since it only depends on the angle of emission and is therefore easy to measure.

A.2 Regions in rapidity space

In the CM frame the two approaching nuclei appear to be Lorentz contracted "pancakes". After they have collided it is possible to distinguish a central region and a fragmentation region (see figure A.1).

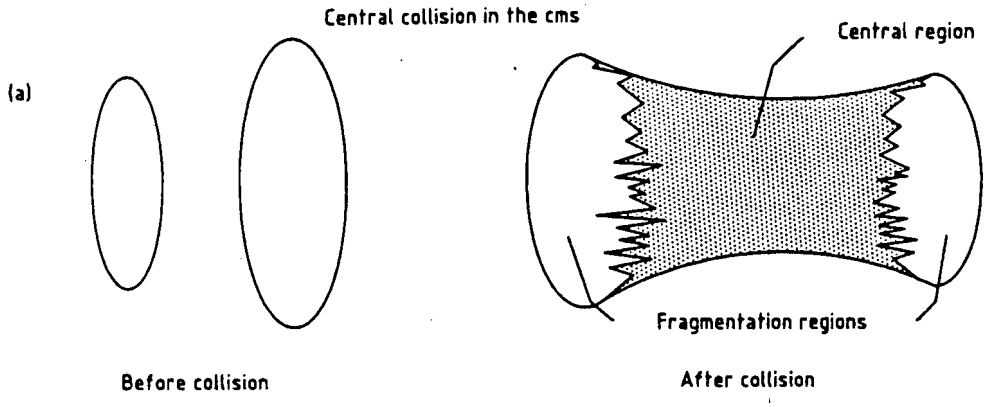

Figure A.1: Two Lorentz contracted nuclei approach each other before a collision. A central region and a fragmentation region remain after the collision [19].

Figure A.2 distinguishes between central and peripheral collisions.

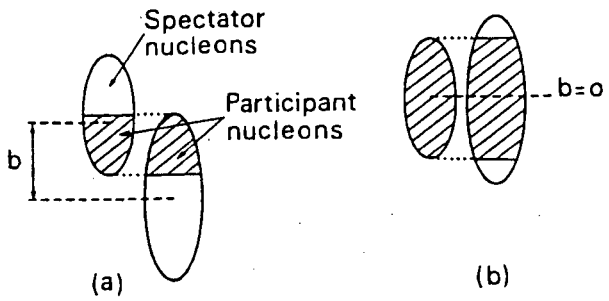

Figure A.2: Peripheral and central collisions in the centre of mass of the two colliding nuclei [35]. b is the impact parameter, quantifying how much of the two colliding nuclei participated in the collision.

Appendix B

A comparison of energies in the CM and lab frames

Consider the Lorentz invariant quantity s in the lab frame and CM frame of a projectile colliding with a stationary target.

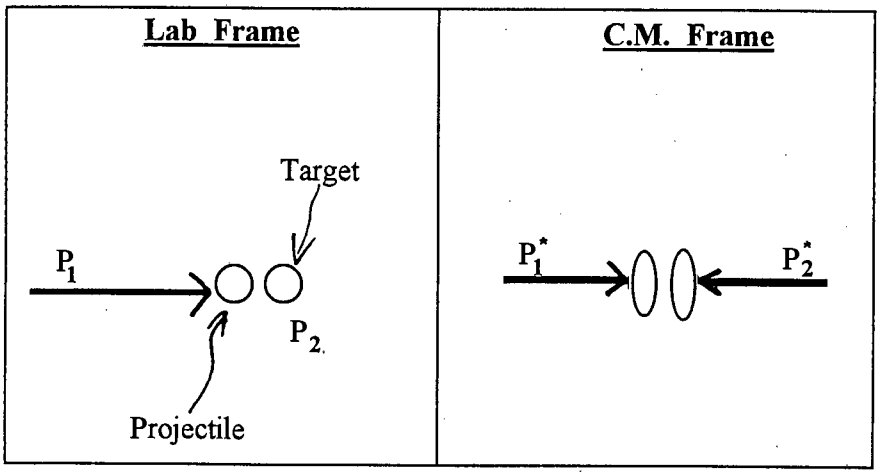

Figure B.1: A projectile colliding with a target, viewed from the lab frame and the CM frame

First we can calculate s in the lab frame:

$$\begin{aligned} s &= (P_1 + P_2)^2 = P_1^2 + P_2^2 + 2P_1 \cdot P_2 \\ &= m_1^2 + m_2^2 + 2E_1^{lab} m_2 \, . \end{aligned}$$

Taking the limit $E_1^{lab} \gg m_1, m_2$,

$$s \approx 2E_1^{lab} m_2 \, . \tag{B.1}$$

Now consider the same collision, viewed from the CM frame:

$$s = (P_1^* + P_2^*)$$

$$= (P_1^0 + P_2^0)^2 - |\vec{p}_1^* + \vec{p}_2^*|^2.$$

Since $|\vec{p}_1^*| = -|\vec{p}_2^*|$ we get:

$$s = (E_1^* + E_2^*)^2 = 4E_1^{*^2}\ , \tag{B.2}$$

assuming that the projectile and the target have the same mass.

Comparing equations B.1 and B.2 one can see:

$$\begin{aligned} 2E_1^{lab}m_2 \quad &= 4E_1^{*^2} \\ \Longrightarrow E_1^* \quad &= \sqrt{\frac{E_1 m_2}{2}}\ . \end{aligned}$$

Thus a beam with an energy of 160MeV/u will translate to 9MeV/u in the CM frame.

Appendix C

A conversion to cylindrical coordinates

A conversion to cylindrical coordinates can be achieved in the following manner. Firstly, d^3p can be transformed into cylindrical coordinates in momentum space:

$$d^3p = d\phi p_T dp_T dp_z \ ,$$

where p_T is the transverse momentum and p_z is the longitudinal momentum. Recalling the definition $m_T^2 = m^2 + p_T^2$, it can be seen that $m_T dm_T = p_T dp_T$ and thus:

$$d^3p = d\phi m_T dm_T dp_z \ . \tag{C.1}$$

Using the definition of rapidity: $y = \tanh^{-1}(p_z/E)$ one can obtain

$$\frac{dy}{dp_z} = \frac{1}{1-\left(\frac{p_z}{E}\right)^2}\left(\frac{E - p_z\frac{dE}{dp_z}}{E^2}\right) \ . \tag{C.2}$$

Substituting

$$\frac{dE}{dp_z} = \frac{p_z}{E}$$

into C.2 and remembering that $E^2 - p_z^2 = m_T^2$, one can obtain:

$$\frac{dy}{dp_z} = \frac{1}{E} \ .$$

Thus $dp_z = Edy$ and substituting this into C.1 we arrive at:

$$d^3p = d\phi m_T dm_T E dy \ .$$

Appendix D

Obtaining an expression for the transverse momentum spectrum

Starting from equation 2.2, we can integrate over rapidity to obtain:

$$\frac{dN}{m_T dm_T} = \frac{gV}{(2\pi)^2} e^{\mu/T} \int_{-\infty}^{\infty} dy m_T \cosh y e^{-(m_T/T)\cosh y} .$$

Using symmetry arguments, we can rewrite the previous equation as:

$$\frac{dN}{m_T dm_T} = \frac{gV}{(2\pi)^2} 2m_T e^{\mu/T} \int_{0}^{\infty} dy \cosh y e^{-(m_T/T)\cosh y} ,$$

and using the definition:

$$K_\nu(z) = \int_0^\infty dt \cosh(\nu(t)) e^{-z\cosh t} ,$$

we can write the transverse momentum spectrum as:

$$\frac{dN}{m_T dm_T} = \frac{gV}{2\pi^2} m_T e^{\mu/T} K_1\left(\frac{m_T}{T}\right) . \tag{D.1}$$

We now consider the limit: $m_T \gg T$, and using the fact that

$$\lim_{z\to\infty} K_1(z) = \sqrt{\frac{\pi}{2z}} e^{-z} ,$$

we find that

$$\lim_{\frac{m_T}{T}\to\infty} K_1\left(\frac{m_T}{T}\right) = \sqrt{\frac{\pi T}{2m_T}} e^{-m_T/T} .$$

Substituting this into equation D.1, we obtain a high m_T limit:

$$\lim_{\frac{m_T}{T}\to\infty} \frac{dN}{m_T dm_T} = \frac{gV}{2\pi} \sqrt{\frac{m_T T}{2\pi}} e^{\mu/T} e^{-m_T/T} . \tag{D.2}$$

Taking the temperature T to be fixed, it is clear that

$$\lim_{\frac{m_T}{T}\to\infty} \frac{dN}{m_T dm_T} \quad \alpha \quad \sqrt{m_T} e^{-m_T/T} .$$

Appendix E

Derivation of the relativistic energy and momentum of a decaying resonance in its rest frame

We start by applying conservation of energy and momentum in the rest frame of the resonance:

$$\begin{aligned} P_R^* &= P_1^* + P_2^* + \cdots + P_n^* \\ \Longrightarrow P_R^* - P_1^* &= P_2^* + \cdots + P_n^* \, . \end{aligned}$$

Squaring both sides and defining:

$$W^2 = \left(\sum_{i=2}^{n} P_i^* \right)^2 \, ,$$

we obtain

$$\begin{aligned} m_R^2 + m_1^2 - 2m_R E_1^* &= W^2 \\ \Longrightarrow E_1^* &= \frac{m_R^2 + m_1^2 - W^2}{2m_R} \, . \end{aligned}$$

Continuing from this expression, we can write:

$$(m_R^2 + m_1^2 - W^2)^2 = 4m_R^2(m_1^2 + |\vec{p}_1^{\,*}|^2) \, .$$

After a little manipulation, we get:

$$|\vec{p}_1^{\,*}|^2 = \frac{1}{4m_R^2} \left(m_R^4 - 2m_R^2 m_1^2 + m_1^4 - 2m_1^2 W^2 - 2m_R^2 W^2 + W^4 \right) \, .$$

Factorising this expression, we end up with:

$$|\vec{p}_1^{\,*}| = \frac{\sqrt{[(m_R + m_1)^2 - W^2][(m_R - m_1)^2 - W^2]}}{2m_R} \, .$$

Appendix F

A particle data table

This table has been compiled from [21]. I designed it for use in calculating pion and kaon spectra from two and three body resonance decays. Heavy resonances which do not make a significant impact ($< 1\%$) on the total spectrum, have been neglected. Notice that some particles are repeated twice since there may be two ways in which the particle in question decays into a pion and some other particle(s). Column 2 gives the spin-isospin degeneracy factor; column 3 gives the mass of the decaying resonance (in GeV); column 4 indicates whether the resonance is a boson or a fermion; column 5 is the strangeness of the resonance, column 6 is the baryon number of the resonance. Columns 7, 8 and 9 are concerned with the two and three body decay of a resonance into a pion and another particle or particles: the mass of the second decay product is given in column 7 (in GeV), the branching ratio of that particular decay channel is given in column 8 and the mass of the second possible decay product is given in column 9. Likewise, columns 10 and 11 give the mass of the other decay product and branching ratio respectively for a resonance decaying into a K^+ and one other particle. Similarly columns 12 and 13 give the relevant information for a resonance decaying into a K^-.

particle	g	M_R	st	S	B	m_2	b($\pi^\pm$)	m_3	m_2	b(K^+)	m_2	b(K^-)
$\pi^\pm$	3	0.139	−1	0	0	0.000	0.000	0.000	0.000	0.000	0.000	0.000
η	1	0.547	−1	0	0	0.139	0.232	0.139	0.000	0.000	0.000	0.000
$\rho(770)$	9	0.768	−1	0	0	0.139	0.667	0.000	0.000	0.000	0.000	0.000
$\omega(782)$	3	0.782	−1	0	0	0.139	0.888	0.139	0.000	0.000	0.000	0.000
$\eta'(958)$	1	0.958	−1	0	0	0.139	0.437	0.547	0.000	0.000	0.000	0.000
$f_0(980)$	1	0.980	−1	0	0	0.139	0.521	0.000	0.000	0.110	0.000	0.110
$a_0(980)$	3	0.983	−1	0	0	0.547	0.300	0.000	0.000	0.167	0.000	0.167
$\phi(1020)$	3	1.019	−1	0	0	0.768	0.086	0.000	0.494	0.491	0.494	0.491
$h_1(1170)$	3	1.170	−1	0	0	0.768	0.333	0.000	0.000	0.000	0.000	0.000

$b_1(1235)$	9	1.231	−1	0	0	0.782	0.300	0.000	0.000	0.000	0.000	0.000
$a_1(1260)$	9	1.230	−1	0	0	0.768	0.300	0.000	0.000	0.000	0.000	0.000
$f_2(1270)$	5	1.275	−1	0	0	0.139	0.565	0.000	0.494	0.023	0.494	0.023
$f_1(1285)$	3	1.282	−1	0	0	0.000	0.000	0.000	0.000	0.000	0.000	0.000
$\eta(1295)$	1	1.295	−1	0	0	0.983	0.167	0.000	0.000	0.000	0.000	0.000
$\pi(1300)$	3	1.300	−1	0	0	0.768	0.167	0.000	0.000	0.000	0.000	0.000
$a_2(1320)$	15	1.318	−1	0	0	0.768	0.234	0.000	0.494	0.025	0.494	0.025
$a_2(1320)$	15	1.318	−1	0	0	0.547	0.048	0.000	0.000	0.000	0.000	0.000
$f_0(1370)$	1	1.370	−1	0	0	0.000	0.000	0.000	0.494	0.071	0.494	0.071
$f_1(1420)$	3	1.427	−1	0	0	0.000	0.000	0.000	0.000	0.000	0.000	0.000
$\omega(1420)$	3	1.419	−1	0	0	0.000	0.000	0.000	0.000	0.000	0.000	0.000
$\eta(1440)$	1	1.415	−1	0	0	0.000	0.000	0.000	0.000	0.000	0.000	0.000
$\rho(1450)$	9	1.465	−1	0	0	0.000	0.000	0.000	0.000	0.000	0.000	0.000
$f_0(1500)$	1	1.503	−1	0	0	0.000	0.000	0.000	0.000	0.000	0.000	0.000
$f_1(1510)$	3	1.512	−1	0	0	0.000	0.000	0.000	0.892	0.250	0.892	0.250
$f_2'(1525)$	5	1.525	−1	0	0	0.000	0.000	0.000	0.494	0.444	0.494	0.444
$\omega(1600)$	3	1.649	−1	0	0	0.000	0.000	0.000	0.000	0.000	0.000	0.000
$\omega_3(1670)$	7	1.667	−1	0	0	0.000	0.000	0.000	0.000	0.000	0.000	0.000
$\pi_2(1670)$	15	1.670	−1	0	0	0.000	0.000	0.000	0.892	0.011	0.892	0.011
$\phi(1680)$	3	1.680	−1	0	0	0.000	0.000	0.000	0.892	0.125	0.892	0.125
$\phi(1680)$	3	1.680	−1	0	0	0.000	0.000	0.000	0.494	0.083	0.494	0.083
$\rho_3(1690)$	21	1.691	−1	0	0	0.000	0.000	0.000	0.494	0.005	0.494	0.005
$\rho_3(1690)$	21	1.691	−1	0	0	0.000	0.000	0.000	0.000	0.000	0.000	0.000
$\rho(1700)$	9	1.700	−1	0	0	0.000	0.000	0.000	0.000	0.000	0.000	0.000
$f_J(1710)$	1	1.697	−1	0	0	0.000	0.000	0.000	0.494	0.167	0.494	0.167
$\phi_3(1850)$	7	1.854	−1	0	0	0.000	0.000	0.000	0.494	0.250	0.494	0.250
$\phi_3(1850)$	7	1.854	−1	0	0	0.000	0.000	0.000	0.892	0.125	0.892	0.125
$f_2(2010)$	5	2.011	−1	0	0	0.000	0.000	0.000	0.000	0.000	0.000	0.000
$f_4(2050)$	9	2.044	−1	0	0	0.000	0.000	0.000	0.000	0.000	0.000	0.000
$f_2(2300)$	5	2.297	−1	0	0	0.000	0.000	0.000	0.000	0.000	0.000	0.000
$f_2(2340)$	5	2.339	−1	0	0	0.000	0.000	0.000	0.000	0.000	0.000	0.000
K^+	2	0.494	−1	1	0	0.000	0.000	0.000	0.000	0.000	0.000	0.000
$K^*(892)$	6	0.892	−1	1	0	0.495	0.333	0.000	0.139	0.500	0.000	0.000
$K_1(1270)$	6	1.273	−1	1	0	0.892	0.053	0.000	0.768	0.210	0.000	0.000
$K_1(1270)$	6	1.273	−1	1	0	0.000	0.000	0.000	0.000	0.055	0.000	0.000
$K_1(1400)$	6	1.402	−1	1	0	0.892	0.313	0.000	0.000	0.000	0.000	0.000
$K^*(1410)$	6	1.412	−1	1	0	0.892	0.167	0.000	0.139	0.033	0.000	0.000
$K_0^*(1430)$	2	1.429	−1	1	0	0.495	0.310	0.000	0.139	0.465	0.000	0.000
$K_2^*(1430)$	10	1.430	−1	1	0	0.495	0.166	0.000	0.139	0.249	0.000	0.000

$K_2^*(1430)$	10	1.430	−1	1	0	0.892	0.084	0.000	0.768	0.044	0.000	0.000
$K^*(1680)$	6	1.714	−1	1	0	0.495	0.129	0.000	0.139	0.194	0.000	0.000
$K^*(1680)$	6	1.714	−1	1	0	0.892	0.100	0.000	0.768	0.157	0.000	0.000
$K_2(1770)$	10	1.773	−1	1	0	1.429	0.167	0.000	1.019	0.063	0.000	0.000
$K_3^*(1780)$	14	1.770	−1	1	0	0.892	0.091	0.000	0.768	0.225	0.000	0.000
$K_3^*(1780)$	14	1.770	−1	1	0	0.495	0.064	0.000	0.139	0.097	0.000	0.000
$K_2(1820)$	10	1.816	−1	1	0	1.429	0.083	0.000	0.782	0.048	0.000	0.000
$K_4^*(2045)$	18	2.045	−1	1	0	0.000	0.000	0.000	0.139	0.050	0.000	0.000
K^-	2	0.494	−1	−1	0	0.000	0.000	0.000	0.000	0.000	0.000	0.000
$K^*(892)$	6	0.892	−1	−1	0	0.495	0.333	0.000	0.000	0.000	0.139	0.500
$K_1(1270)$	6	1.273	−1	−1	0	0.892	0.053	0.000	0.000	0.000	0.768	0.210
$K_1(1270)$	6	1.273	−1	−1	0	0.000	0.000	0.000	0.000	0.000	0.000	0.055
$K_1(1400)$	6	1.402	−1	−1	0	0.892	0.313	0.000	0.000	0.000	0.000	0.000
$K^*(1410)$	6	1.412	−1	−1	0	0.892	0.167	0.000	0.000	0.000	0.139	0.033
$K_0^*(1430)^-$	2	1.429	−1	−1	0	0.495	0.310	0.000	0.000	0.000	0.139	0.465
$K_2^*(1430)$	10	1.430	−1	−1	0	0.495	0.166	0.000	0.000	0.000	0.139	0.249
$K_2^*(1430)$	10	1.430	−1	−1	0	0.892	0.084	0.000	0.000	0.000	0.768	0.044
$K^*(1680)$	6	1.714	−1	−1	0	0.495	0.129	0.000	0.000	0.000	0.139	0.194
$K^*(1680)$	6	1.714	−1	−1	0	0.892	0.100	0.000	0.000	0.000	0.768	0.157
$K_2(1770)$	10	1.773	−1	−1	0	1.429	0.167	0.000	0.000	0.000	1.019	0.063
$K_3^*(1780)$	14	1.770	−1	−1	0	0.892	0.091	0.000	0.000	0.000	0.768	0.225
$K_3^*(1780)$	14	1.770	−1	−1	0	0.495	0.064	0.000	0.000	0.000	0.139	0.097
$K_2(1820)$	10	1.816	−1	−1	0	1.429	0.083	0.000	0.000	0.000	0.782	0.048
$K_4^*(2045)$	18	2.045	−1	−1	0	0.000	0.000	0.000	0.000	0.000	0.139	0.050
p/n	4	0.939	1	0	1	0.000	0.000	0.000	0.000	0.000	0.000	0.000
$N(1440)$	4	1.440	1	0	1	0.939	0.200	0.000	0.000	0.000	0.000	0.000
$N(1440)$	4	1.440	1	0	1	1.232	0.067	0.000	0.000	0.000	0.000	0.000
$N(1520)$	8	1.520	1	0	1	0.939	0.183	0.000	0.000	0.000	0.000	0.000
$N(1520)$	8	1.520	1	0	1	1.232	0.083	0.000	0.000	0.000	0.000	0.000
$N(1535)$	4	1.535	1	0	1	0.939	0.133	0.000	0.000	0.000	0.000	0.000
$N(1650)$	4	1.650	1	0	1	0.000	0.000	0.000	0.000	0.000	0.000	0.000
$N(1675)$	12	1.675	1	0	1	0.000	0.000	0.000	0.000	0.000	0.000	0.000
$N(1680)$	12	1.680	1	0	1	0.000	0.000	0.000	0.000	0.000	0.000	0.000
$N(1700)$	8	1.700	1	0	1	0.000	0.000	0.000	0.000	0.000	0.000	0.000
$N(1710)$	4	1.710	1	0	1	0.000	0.000	0.000	0.000	0.000	0.000	0.000
$N(1720)$	8	1.720	1	0	1	0.000	0.000	0.000	0.000	0.000	0.000	0.000
$N(2190)$	16	2.190	1	0	1	0.000	0.000	0.000	0.000	0.000	0.000	0.000
$N(2220)$	20	2.220	1	0	1	0.000	0.000	0.000	0.000	0.000	0.000	0.000
$N(2250)$	20	2.250	1	0	1	0.000	0.000	0.000	0.000	0.000	0.000	0.000
$N(2600)$	24	2.600	1	0	1	0.000	0.000	0.000	0.000	0.000	0.000	0.000

$\Delta(1232)$	16	1.232	1	0	1	0.939	0.331	0.000	0.000	0.000	0.000	0.000
$\Delta(1600)$	16	1.600	1	0	1	0.939	0.058	0.000	0.000	0.000	0.000	0.000
$\Delta(1600)$	16	1.600	1	0	1	1.232	0.133	0.000	0.000	0.000	0.000	0.000
$\Delta(1620)$	8	1.620	1	0	1	0.000	0.000	0.000	0.000	0.000	0.000	0.000
$\Delta(1700)$	16	1.700	1	0	1	0.000	0.000	0.000	0.000	0.000	0.000	0.000
$\Delta(1900)$	8	1.900	1	0	1	0.000	0.000	0.000	0.000	0.000	0.000	0.000
$\Delta(1905)$	24	1.905	1	0	1	0.000	0.000	0.000	0.000	0.000	0.000	0.000
$\Delta(1910)$	8	1.910	1	0	1	0.000	0.000	0.000	0.000	0.000	0.000	0.000
$\Delta(1920)$	16	1.920	1	0	1	0.000	0.000	0.000	0.000	0.000	0.000	0.000
$\Delta(1930)$	24	1.930	1	0	1	0.000	0.000	0.000	0.000	0.000	0.000	0.000
$\Delta(1950)$	32	1.950	1	0	1	0.000	0.000	0.000	0.000	0.000	0.000	0.000
$\Delta(2420)$	48	2.420	1	0	1	0.000	0.000	0.000	0.000	0.000	0.000	0.000
Λ	2	1.116	1	-1	1	0.000	0.000	0.000	0.000	0.000	0.000	0.000
$\Lambda(1405)$	2	1.407	1	-1	1	1.192	0.333	0.000	0.000	0.000	0.000	0.000
$\Lambda(1520)$	4	1.519	1	-1	1	1.192	0.140	0.000	0.000	0.000	0.939	0.225
$\Lambda(1600)$	2	1.600	1	-1	1	1.192	0.117	0.000	0.000	0.000	0.939	0.120
$\Lambda(1670)$	2	1.670	1	-1	1	1.192	0.133	0.000	0.000	0.000	0.939	0.100
$\Lambda(1690)$	4	1.690	1	-1	1	1.192	0.100	0.000	0.000	0.000	0.939	0.125
$\Lambda(1800)$	2	1.800	1	-1	1	0.000	0.000	0.000	0.000	0.000	0.939	0.163
$\Lambda(1810)$	2	1.810	1	-1	1	0.000	0.000	0.000	0.000	0.000	0.939	0.175
$\Lambda(1820)$	6	1.820	1	-1	1	0.000	0.000	0.000	0.000	0.000	0.939	0.300
$\Lambda(1830)$	6	1.830	1	-1	1	0.000	0.000	0.000	0.000	0.000	0.939	0.033
$\Lambda(1890)$	4	1.890	1	-1	1	0.000	0.000	0.000	0.000	0.000	0.939	0.138
$\Lambda(2100)$	8	2.100	1	-1	1	0.000	0.000	0.000	0.000	0.000	0.000	0.000
$\Lambda(2110)$	6	2.110	1	-1	1	0.000	0.000	0.000	0.000	0.000	0.000	0.000
$\Lambda(2350)$	10	2.350	1	-1	1	0.000	0.000	0.000	0.000	0.000	0.000	0.000
$\Sigma^{\pm}$	6	1.192	1	-1	1	0.000	0.000	0.000	0.000	0.000	0.000	0.000
$\Sigma(1385)$	12	1.385	1	-1	1	1.116	0.293	0.000	0.000	0.000	0.000	0.000
$\Sigma(1385)$	12	1.385	1	-1	1	1.192	0.040	0.000	0.000	0.000	0.000	0.000
$\Sigma(1660)$	6	1.660	1	-1	1	1.116	0.133	0.000	0.000	0.000	0.939	0.100
$\Sigma(1660)$	6	1.660	1	-1	1	1.192	0.133	0.000	0.000	0.000	0.000	0.000
$\Sigma(1670)$	12	1.670	1	-1	1	1.116	0.033	0.000	0.000	0.000	0.939	0.050
$\Sigma(1670)$	12	1.670	1	-1	1	1.192	0.150	0.000	0.000	0.000	0.000	0.000
$\Sigma(1750)$	6	1.750	1	-1	1	0.000	0.000	0.000	0.000	0.000	0.939	0.125
$\Sigma(1775)$	18	1.775	1	-1	1	0.000	0.000	0.000	0.000	0.000	0.939	0.100
$\Sigma(1915)$	18	1.915	1	-1	1	0.000	0.000	0.000	0.000	0.000	0.000	0.000
$\Sigma(1940)$	12	1.940	1	-1	1	0.000	0.000	0.000	0.000	0.000	0.000	0.000
$\Sigma(2030)$	24	2.030	1	-1	1	0.000	0.000	0.000	0.000	0.000	0.000	0.000
Ξ^{-}	4	1.320	1	-2	1	0.000	0.000	0.000	0.000	0.000	0.000	0.000
$\Xi(1530)$	8	1.530	1	-2	1	1.320	0.333	0.000	0.000	0.000	0.000	0.000

$\Xi(1820)$	8	1.823	1	-2	1	0.000	0.000	0.000	0.000	0.000	0.000	0.000
$\Xi(2030)$	12	2.025	1	-2	1	0.000	0.000	0.000	0.000	0.000	0.000	0.000
Ω^-	4	1.672	1	-3	1	0.000	0.000	0.000	0.000	0.000	0.000	0.000
$\bar{p}/\bar{n}$	4	0.939	1	0	-1	0.000	0.000	0.000	0.000	0.000	0.000	0.000
$\bar{N}(1440)$	4	1.440	1	0	-1	0.939	0.200	0.000	0.000	0.000	0.000	0.000
$\bar{N}(1440)$	4	1.440	1	0	-1	1.232	0.067	0.000	0.000	0.000	0.000	0.000
$\bar{N}(1520)$	8	1.520	1	0	-1	0.939	0.183	0.000	0.000	0.000	0.000	0.000
$\bar{N}(1520)$	8	1.520	1	0	-1	1.232	0.083	0.000	0.000	0.000	0.000	0.000
$\bar{N}(1535)$	4	1.535	1	0	-1	0.939	0.133	0.000	0.000	0.000	0.000	0.000
$\bar{N}(1650)$	4	1.650	1	0	-1	0.000	0.000	0.000	0.000	0.000	0.000	0.000
$\bar{N}(1675)$	12	1.675	1	0	-1	0.000	0.000	0.000	0.000	0.000	0.000	0.000
$\bar{N}(1680)$	12	1.680	1	0	-1	0.000	0.000	0.000	0.000	0.000	0.000	0.000
$\bar{N}(1700)$	8	1.700	1	0	-1	0.000	0.000	0.000	0.000	0.000	0.000	0.000
$\bar{N}(1710)$	4	1.710	1	0	-1	0.000	0.000	0.000	0.000	0.000	0.000	0.000
$\bar{N}(1720)$	8	1.720	1	0	-1	0.000	0.000	0.000	0.000	0.000	0.000	0.000
$\bar{N}(2190)$	16	2.190	1	0	-1	0.000	0.000	0.000	0.000	0.000	0.000	0.000
$\bar{N}(2220)$	20	2.220	1	0	-1	0.000	0.000	0.000	0.000	0.000	0.000	0.000
$\bar{N}(2250)$	20	2.250	1	0	-1	0.000	0.000	0.000	0.000	0.000	0.000	0.000
$\bar{N}(2600)$	24	2.600	1	0	-1	0.000	0.000	0.000	0.000	0.000	0.000	0.000
$\bar{\Delta}(1232)$	16	1.232	1	0	-1	0.939	0.331	0.000	0.000	0.000	0.000	0.000
$\bar{\Delta}(1600)$	16	1.600	1	0	-1	0.939	0.058	0.000	0.000	0.000	0.000	0.000
$\bar{\Delta}(1600)$	16	1.600	1	0	-1	1.232	0.133	0.000	0.000	0.000	0.000	0.000
$\bar{\Delta}(1620)$	8	1.620	1	0	-1	0.000	0.000	0.000	0.000	0.000	0.000	0.000
$\bar{\Delta}(1700)$	16	1.700	1	0	-1	0.000	0.000	0.000	0.000	0.000	0.000	0.000
$\bar{\Delta}(1900)$	8	1.900	1	0	-1	0.000	0.000	0.000	0.000	0.000	0.000	0.000
$\bar{\Delta}(1905)$	24	1.905	1	0	-1	0.000	0.000	0.000	0.000	0.000	0.000	0.000
$\bar{\Delta}(1910)$	8	1.910	1	0	-1	0.000	0.000	0.000	0.000	0.000	0.000	0.000
$\bar{\Delta}(1920)$	16	1.920	1	0	-1	0.000	0.000	0.000	0.000	0.000	0.000	0.000
$\bar{\Delta}(1930)$	24	1.930	1	0	-1	0.000	0.000	0.000	0.000	0.000	0.000	0.000
$\bar{\Delta}(1950)$	32	1.950	1	0	-1	0.000	0.000	0.000	0.000	0.000	0.000	0.000
$\bar{\Delta}(2420)$	48	2.420	1	0	-1	0.000	0.000	0.000	0.000	0.000	0.000	0.000
$\bar{\Lambda}$	2	1.116	1	1	-1	0.000	0.000	0.000	0.000	0.000	0.000	0.000
$\bar{\Lambda}(1405)$	2	1.407	1	1	-1	1.192	0.333	0.000	0.000	0.000	0.000	0.000
$\bar{\Lambda}(1520)$	4	1.519	1	1	-1	1.192	0.140	0.000	0.939	0.225	0.000	0.000
$\bar{\Lambda}(1600)$	2	1.600	1	1	-1	1.192	0.117	0.000	0.939	0.120	0.000	0.000
$\bar{\Lambda}(1670)$	2	1.670	1	1	-1	1.192	0.133	0.000	0.939	0.100	0.000	0.000
$\bar{\Lambda}(1690)$	4	1.690	1	1	-1	1.192	0.100	0.000	0.939	0.125	0.000	0.000
$\bar{\Lambda}(1800)$	2	1.800	1	1	-1	0.000	0.000	0.000	0.939	0.163	0.000	0.000
$\bar{\Lambda}(1810)$	2	1.810	1	1	-1	0.000	0.000	0.000	0.939	0.175	0.000	0.000
$\bar{\Lambda}(1820)$	6	1.820	1	1	-1	0.000	0.000	0.000	0.939	0.300	0.000	0.000

$\bar{\Lambda}(1830)$	6	1.830	1	1	-1	0.000	0.000	0.000	0.939	0.033	0.000	0.000
$\bar{\Lambda}(1890)$	4	1.890	1	1	-1	0.000	0.000	0.000	0.939	0.138	0.000	0.000
$\bar{\Lambda}(2100)$	8	2.100	1	1	-1	0.000	0.000	0.000	0.000	0.000	0.000	0.000
$\bar{\Lambda}(2110)$	6	2.110	1	1	-1	0.000	0.000	0.000	0.000	0.000	0.000	0.000
$\bar{\Lambda}(2350)$	10	2.350	1	1	-1	0.000	0.000	0.000	0.000	0.000	0.000	0.000
$\bar{\Sigma}^{\pm}$	6	1.192	1	1	-1	0.000	0.000	0.000	0.000	0.000	0.000	0.000
$\bar{\Sigma}(1385)$	12	1.385	1	1	-1	1.116	0.293	0.000	0.000	0.000	0.000	0.000
$\bar{\Sigma}(1385)$	12	1.385	1	1	-1	1.192	0.040	0.000	0.000	0.000	0.000	0.000
$\bar{\Sigma}(1660)$	6	1.660	1	1	-1	1.116	0.133	0.000	0.939	0.100	0.000	0.000
$\bar{\Sigma}(1660)$	6	1.660	1	1	-1	1.192	0.133	0.000	0.000	0.000	0.000	0.000
$\bar{\Sigma}(1670)$	12	1.670	1	1	-1	1.116	0.033	0.000	0.939	0.050	0.000	0.000
$\bar{\Sigma}(1670)$	12	1.670	1	1	-1	1.192	0.150	0.000	0.000	0.000	0.000	0.000
$\bar{\Sigma}(1750)$	6	1.750	1	1	-1	0.000	0.000	0.000	0.939	0.125	0.000	0.000
$\bar{\Sigma}(1775)$	18	1.775	1	1	-1	0.000	0.000	0.000	0.939	0.100	0.000	0.000
$\bar{\Sigma}(1915)$	18	1.915	1	1	-1	0.000	0.000	0.000	0.000	0.000	0.000	0.000
$\bar{\Sigma}(1940)$	12	1.940	1	1	-1	0.000	0.000	0.000	0.000	0.000	0.000	0.000
$\bar{\Sigma}(2030)$	24	2.030	1	1	-1	0.000	0.000	0.000	0.000	0.000	0.000	0.000
$\bar{\Xi}$	4	1.320	1	2	-1	0.000	0.000	0.000	0.000	0.000	0.000	0.000
$\bar{\Xi}(1530)$	8	1.530	1	2	-1	1.320	0.333	0.000	0.000	0.000	0.000	0.000
$\bar{\Xi}(1820)$	8	1.823	1	2	-1	0.000	0.000	0.000	0.000	0.000	0.000	0.000
$\bar{\Xi}(2030)$	12	2.025	1	2	-1	0.000	0.000	0.000	0.000	0.000	0.000	0.000
$\bar{\Omega}$	4	1.672	1	3	-1	0.000	0.000	0.000	0.000	0.000	0.000	0.000

Bibliography

[1] J. Sollfrank, P. Koch and U. Heinz, *The influence of resonance decays on the p_T spectra from heavy-ion collisions.* Phys. Lett. B **252**, 256 (1990).

[2] G. Agakichiev *et. al.*, *Enhanced Production of Low-Mass Electron Pairs in 200GeV/ Nucleon S-Au Collisions at the CERN Super Proton Synchrotron* Phys. Rev. Lett. **75**, 1272 (1995).

[3] J. Sollfrank, P. Koch and U. Heinz, *Is there a low p_T "anomaly" in the pion momentum spectra from relativistic nuclear collisions?* Z Phys. C **52**, 593 (1991).

[4] G. E. Brown, J. Stachel and G. M. Welke, *Pions from resonance decay in Brookhaven relativistic heavy-ion collisions* Phys. Lett. B **253**, 19 (1991).

[5] H. W. Barz *et. al.*, *The transverse momentum spectrum in ultrarelativistic heavy ion collisions is not statistical* Phys. Lett. B **254**, 332 (1991).

[6] J. Rafelski, *Formation and observation of the quark-gluon plasma* Phys. Reports **88**, 331 (1982).

[7] E.V. Shuryak, *Quark-gluon plasma and hadronic production of leptons, photons and psions* Phys. Lett. **78B**, 150 (1978).

[8] T. Matsui and H. Satz, *J/Ψ suppression by quark-gluon plasma formation* Phys. Lett. B **178**, 416 1986.

[9] E. Schnedermann, J. Sollfrank and U. Heinz, *Thermal phenomenology of hadrons from 200A GeV S+S collisions* Phys. Rev. C **48**, 2462 (1993).

[10] G. Odyniec, *Similarities and differences in strangeness production at BNL and CERN*, in [32] p.399.

[11] J. Bjorken, *Highly relativistic nucleus-nucleus collisions: The central rapidity region* Phys. Rev. D **27**, 140 (1983).

[12] G. Baym *et. al.*, *Hydrodynamics of ultra-relativistic heavy ion collisions* Nuclear Phys. **A407**, 541 (1983).

[13] *Quark Matter '96*, edited by P. Braun-Munzinger *et. al.* [Nucl. Phys. **A610** (1996)].

[14] M. Gonin *et. al.*, NA50 collaboration, *Observation of threshold effects in the J/Ψ anomalous suppression for Pb+Pb collisions at CERN* presented at RHIC '97.

[15] *Thermal Physics*, C. Kittel and H. Kroemer. [W. H. Freeman and Company, second edition (1980)]

[16] *Table of Integrals, Series, and Products*, I. S. Gradshteyn and I. M. Ryzhik, edited by A. Jeffrey [Academic Press (1994)].

[17] D. M. Elliott, M.Sc. thesis, University of Cape Town, 1996.

[18] A. Muronga, M.Sc. thesis, University of Cape Town, 1996.

[19] M. Marais, M.Sc. thesis, University of Cape Town, 1997.

[20] *Quarks and Leptons: An Introductory Course in Modern Particle Physics*, F. Halzen and A. D. Martin [John Wiley & Sons (1984)].

[21] *Review of Particle Physics*, edited by E.J. Weinberg *et. al.* Phys. Rev. D **54** (1996).

[22] F. Cooper and G. Frye, *Single-particle distribution in the hydrodynamic and statistical thermodynamic models of multiparticle production* Phys. Rev. D **10**, 186 (1974).

[23] F. Grassi, Y. Hama and T. Kodama, *Particle emission in the hydrodynamical description of relativistic nuclear collisions* Z. Phys. C **73**, 153 (1996).

[24] I. G. Bearden *et. al.*, *Collective expansion in high energy heavy ion collisions* Phys. Rev. Lett. **78**, 2080 (1997).

[25] K. S. Lee, U. Heinz and E. Schnedermann, *Search for collective transverse flow using particle transverse momentum spectra in relativistic heavy-ion collisions* Z. Phys. C **48**, 525 (1990).

[26] Yu. M. Sinyukov, V.A. Averchenkov and B. Lörstad, *Interferometrical signature of mixed phase in A+A collisions* Z. Phys. C **49**, 417 (1991).

[27] Bao-An Li and Wolfgang Bauer, *Two-temperature shape of pion spectra in relativistic heavy-ion reactions* Phys. Lett. B **254**, 335 (1991).

[28] M. Kataja and P. V. Ruuskanen, *Non-zero chemical potential and the shape of the p_T distribution of hadrons in heavy-ion collisions* Phys. Lett. B **243**, 181 (1990).

[29] E. V. Shuryak, *The "soft photon puzzle" and pion modification in hadronic matter* Phys. Lett. B **231**, 175 (1989).

[30] *Private discussions with Prof. J. Cleymans.*

[31] *Private discussions with D. M. Elliott*

[32] *Hot hadronic matter, theory and experiment*, edited by J. Letessier *et. al.* [Plenum Press (1995)].

[33] R. Hagedorn, *The long way to the statistical bootstrap model*, in [32] p.13.

[34] V. F. Weisskopf, Phys. Rev. **52**, 295 (1937).

[35] R. A. Salmeron, *An introduction to the search for the quark-gluon plasma in ultra-relativistic heavy ion interactions*

[36] P. J. Siemens and J. O. Rasmussen, *Evidence for a blast wave from compressed nuclear matter* Phys. Rev. Lett. **42**, 880 (1979).

[37] S. V. Åfanasiev *et. al.*, *Hadron yields and hadron spectra from the NA49 experiment* in *Quark Matter '96* [13], p.188c.

Index

Acknowledgements

Grateful thanks must go first to my supervisor, Prof. J. Cleymans. He is a physicist in the true sense of the word, able to find physical meaning in the most obscure theories. His ability to elucidate the most difficult concepts in the simplest terms made for enjoyable and enlightening discussions.

Thanks to Duncan Elliott for aggressive support, correcting my spelling, grammar and shortening my sentences. Thank you as well for many interesting discussions.

Thank you to the Foundation for Research and Development for providing me with financial support.

Thanks to Jonathan Beattie for many hours spent over a pool table and for sharing in the discovery of the finer arts of the game.

Particular thanks must go to Dr. R. Fearick and Mrs. J. Parsons for aiding me in my quest for mastery over LaTeX.

Special thanks to Douw Steyn for giving up many hours of his time, to explain the art of Fortran programming and helping me with LaTeX.

Thanks to my parents for their support, both financial and moral. Without them, I would not be where I am today. Their hard work and dedication has been an inspiration.

Thank you to Ian Fairweather for proof reading this thesis.

Finally thank you to the Dawsons for many fine meals. Thanks to Louise for reminders of wonderment and studentship, for patiently teaching me new things and trying very hard to understand my poor explanations of physics.